THE JOURNAL OF Ammonia Energy

Available online at

jae.cardiffuniversitypress.org

ISSN **2752-7735**
The Journal of Ammonia Energy 02 (2024) 042–063

Cardiff University Press | Gwasg Prifysgol Caerdydd

A computational study of the use of hydrogen peroxide as pilot fuel for a homogeneous mixture of ammonia/hydrogen in a compression ignition engine

Tingas E-A[a*], Hardalupas Y[b], Taylor AMKP[b]

[a]*School of Computing, Engineering and the Built Environment, Edinburgh Napier University, Edinburgh, EH10 5DT, UK*
[b]*Department of Mechanical Engineering, Imperial College London, Exhibition Rd, London SW7 2AZ, UK*

Abstract

We report a computational investigation of a compression ignition (CI) engine (compression ratio: 17.6, displacement volume: 1.3 L) where the main fuel is a homogeneous mixture of ammonia (70-60% vol%) and hydrogen (30-40% vol%), with a global equivalence ratio varying between 0.44 and 0.5, depending on the H_2/NH_3 ratio. The novelty of this study is that it employs a pilot injection of hydrogen peroxide to initiate ignition, without the use of any air or charge preheating (the temperature/pressure at intake BDC are 330 K/1.4 atm, representing mild boost and efficient intercooling). Hydrogen peroxide (H_2O_2) has the attributes that it can be produced from renewable sources, and it is already widely manufactured, distributed, and stored, with diverse applications (as an aqueous solution of H_2O_2 with shares up to 30 vol%). The main advantage of using H_2O_2 as pilot fuel, as opposed to other more conventional ones (*e.g.*, diesel), is that it contains no carbon, and hence produces no CO_2 and particulate matter (PM). The computational investigation was conducted with an advanced commercial stochastic reactor engine model that has been previously validated. The investigation was primarily focused on assessing the effects of using hydrogen peroxide in aqueous solution as pilot fuel on engine efficiency, combustion phasing and NO_x emissions. These three aspects were investigated over a range of engine speeds (750-1,750 rpm) in view of: (i) the variation of the mass of the directly injected (DI) aqueous solution (0.1-10.0 mg); (ii) the variation of the H_2O_2 share (15-50%) in the directly injected (DI) aqueous solution; (iii) the variation of the start of injection (from -20 to -4 CAD aTDC) and injection duration (1-8 CAD). There is a strong effect of the peroxide in advancing combustion timing (CAD50 is advanced by up to 15 CAD) and in decreasing combustion duration (CAD90-CAD10 decreases up to 10 CAD), and peroxide readily enables medium engine loads which are the ones investigated in this work. Indicated thermal efficiencies above 50% were readily achieved at all engine speeds and, with a 30 vol% peroxide share in the solution, the pressure rise rate was always below 30 bar/ms. However, the NO_x emissions in all cases exceeded the International Maritime Organization's Tier III standard. Possible ways to tackle this would be either the use of exhaust gas recirculation, the optimisation of the injection strategy, or the use of aftertreatment. Ammonia slip was negligibly small, yet the greenhouse gas N_2O emissions were found in most cases to be relatively high, consistent with other relevant approaches reported in the literature. For most cases, on a volume basis, the required aqueous H_2O_2 amounts to 3% of the main fuel blend, while on an energy basis this translates to 1.1% of the main fuel blend. The results reported in this initial study are promising because it is possible to ignite a premixed charge on the basis of a small pilot volume of commercially available hydrogen peroxide solution. Engine experiments are necessary to provide further insight into the proposed technology and corroboration of the calculations reported herein.

Selection and/or peer-review under responsibility of Cardiff University

Received: 17th Dec 23; Accepted: 8th April 24; Published: 4th Jul 24

Keywords: zero-carbon engine, hydrogen peroxide, ignition promoter, CI engine, heavy-duty engine.

Introduction

The use of ammonia as a fuel has been advocated by many as a potentially viable route for the decarbonization of heavy-duty applications where the use of batteries or fuel cells is considered either economically unviable or impractical [1-5]. One of these applications currently being explored by industry and academia as a particularly attractive solution is in the maritime sector [6-8]. Marine engines (both the low speed two stroke used in long haul ocean-going ships, and the medium and high-speed engines used as auxiliary power for *e.g.* "hotel" loads) are predominantly of the compression ignition (CI) type where the ignition of the charge is controlled by the direct injection of hydrocarbon fuels just before the top dead center (TDC). The use of ammonia in such engines is primarily hampered

* Corresponding author. E-mail address: e.tingas@napier.ac.uk
https://doi.org/10.18573/jae.28

by ammonia's high autoignition temperature. Its poor reactivity and low flame speed pose additional constraints in its use, especially for medium and high-speed engines, problems that need to be addressed. To mitigate these challenges, even if only partly, the mixing of ammonia with hydrogen has been proposed, a strategy which leverages the ability to produce the required quantity of hydrogen on site through cracking of the bunkered ammonia. Hydrogen has significantly higher flame speed and is much more reactive under engine relevant conditions. Nevertheless, its autoignition temperature is also substantially higher than the one required for its use in conventional CI engines [9]. Therefore, ammonia/hydrogen mixtures still suffer from high autoignition temperatures, thereby posing a challenge for their use in CI engines.

To circumvent these issues, three approaches have been proposed in the literature [10]. The first entails the increase of the compression ratio to sufficiently high values. Previous studies have reported that the use of pure ammonia requires compression ratios above 35:1 combined with substantial preheating [10]. Such compression ratios are not only much higher than those used in current conventional CI engines, which typically operate in the range of 15:1 – 22:1, but also the use of such compression ratios would have prohibitively high frictional losses.

The second approach involves air preheating (or charge) to sufficiently high values [10]. This is conceptually a simple approach and there are a few studies in the literature that have reported promising results. Pochet et al. [11] used ammonia/hydrogen blends in a homogeneous charge compression ignition (HCCI) engine to investigate the production of NO_x emissions as a function of the ammonia share. They managed to achieve stable combustion using 1.5 bar intake pressure and 473 K intake temperature but highlighted the need to minimise the intake temperature in order to maximise power and the use of exhaust gas recirculation (EGR) to tackle NO_x emissions. The same group later used a different HCCI engine with a compression ratio of 22:1 and an intake temperature of 513 K [12]. Their work corroborated the need of EGR to effectively reduce NO_x emissions. However, the use of EGR came with the caveat of increased N_2O emissions (a potent greenhouse gas) and the authors concluded that the combustion temperature needs to be maintained significantly above 1,400 K to ensure low levels of N_2O production. Wang et al. [13] used a conventional CI engine with enhanced air preheating (551K) to investigate the optimal compression ratio (from 13.5:1 to 16.5:1) and injection strategy for different ammonia/hydrogen blends. The rationale for incorporating hydrogen into the primary fuel mix stems from its potential to diminish the necessity to preheat the charge. This is due to hydrogen's lower autoignition temperature and increased reactivity relative to ammonia. Moreover, this rationale was bolstered by the utilization of hydrogen cracked from ammonia, thus establishing a logistical dependence solely on ammonia for routine engine operations. [10]. The authors reported that the delay of the injection timing leads to power reduction and NO_x decrease, while the increase of the compression ratio can lead to improvement of power accompanied by the progressive increase of NO_x emissions. The same group used the numerical approach proposed in Ref. [13] to investigate the effect of different inlet temperatures (476K–551K) and different ammonia/hydrogen blends on the engine's power output and emissions [14]. The authors reported that in all cases the increase of the inlet temperature has a considerable detrimental effect on the engine power, the fuel consumption and NO_x emissions, while augmenting the hydrogen share increases the risk for abnormal engine operation. These findings underscore the importance of optimizing engine performance by minimizing the need for enhanced inlet temperature while also limiting the need for hydrogen in the fuel mix to the bare minimum.

An alternative and possibly more attractive approach to air preheating is the use of a dual fuel concept, where the ignition of the (low reactivity) ammonia (or ammonia-hydrogen mixture) fuel is accomplished by using a (high reactivity) pilot fuel, a fuel with a conveniently lower autoignition temperature [10, 15]. In most studies reported in the literature it is diesel that is used as pilot fuel. Wang et al. [16] investigated numerically the effect of different ammonia/hydrogen blends on the engine power, combustion phasing and emissions. One of the key conclusions of their research was that the optimal ammonia/hydrogen blend at the examined conditions was 7:3 on a mass basis, but they highlighted that even at these conditions, NO_x emissions increase significantly with the increase of the inlet temperature. The same group investigated different injection strategies for the ammonia/hydrogen blends and diesel, and identified a combination of a suitable injection strategy and ammonia/hydrogen blend that reduced, significantly, ammonia slip and N_2O production [17]. Nevertheless, the authors reported that NO_x emissions remain high, exceeding the emission standards of the International Maritime Organization's (IMO) Tier III.

Although using diesel as pilot is a reasonable approach as it allows the use of the vast established knowledge and practical experience on its effective use, it results in the emission of greenhouse gases

(GHG) and soot. An alternative solution that is free of any carbon atoms is to use hydrogen peroxide (H_2O_2) as an ignition promoter. Hydrogen peroxide is a compound which is widely manufactured, distributed, and stored, with diverse applications ranging from medical use to processing and bleaching certain foods and as a domestic cleaner and disinfectant. Although the literature on the use of hydrogen peroxide in combustion engines is limited, recent academic research has corroborated its potential as an ignition promoter in combination with different fuels, such as diesel [18–20], hydrogen [21-22], butanol [23], and ammonia [24-25]. Shafiq and Tingas [24] investigated a combination of ammonia and hydrogen peroxide blends in an HCCI engine model, showing a power increase of 65% and a nine-fold decrease in NO_x emissions compared to the use of an adequately preheated ammonia/air charge, demonstrating the potential of the promoter with ammonia. However, they also demonstrated that the required aqueous hydrogen peroxide would need to be between 20 and 40% of the ammonia volume to achieve ignition, thereby indicating that its use as pilot fuel would potentially be more valuable if ammonia were to be mixed with hydrogen. Dimitrova et al. [22] concluded that H_2/H_2O_2 blends can improve engine performance and thermal efficiency while reducing NO_x emissions in an HCCI engine. Zhou et al. [23] used an aqueous solution of H_2O_2 (30% vol%) in an HCCI engine fuelled with butanol, demonstrating that commercially available peroxide concentrations could be used as a promoter, potentially world-wide and even at higher concentrations if needed in engine operations.

In the current work, an extensive computational campaign is undertaken using aqueous H_2O_2 solutions as a pilot fuel for a NH_3/H_2 fuelled CI engine. This approach also has the operational advantage that it eliminates completely the need for preheating the air (or the NH_3/H_2 charge) while also permitting operation at very lean conditions (equivalence ratios ranging between 0.44 and 0.5). The objective of the current computational study, using an advanced stochastic engine model, is to evaluate the effect of the use of the solution as pilot fuel on the engine performance, combustion phasing and NO_x emissions. This objective is accomplished as a function of: (i) the mass of the directly injected solution; (ii) the share of H_2O_2 in the directly injected mass solution; (iii) different injection strategies, namely by varying the start of injection (SOI) and the injection duration (ID). The knowledge from the current work provides valuable guidance and insight for future engine experiments to verify the proposed technology and evaluate our computational methodology.

Materials and Methods

The setup that is used in the current study represents a four-stroke IVECO engine and the specifications of the engine are summarised in Table 1 for conventional operation with diesel fuel. The engine has been previously used successfully in a dual-fuel mode with natural gas and diesel as the low and high reactivity fuels, respectively [26].

In the current work, a stochastic reactor model (CMCL Innovations MoDS-SRM Engine Suite v2021) has been employed which has been successfully used in other engine studies, e.g., [27–30]. A detailed description of the mathematical formulation of the setup can be found in Ref. [31]. Briefly, the employed engine model solves a joint scalar Probability Density Function (PDF) transport equation [32] using a stochastic numerical method. The model assumes that the contents of the reactor are statistically homogeneous which means that the probability of any property (*e.g.*, temperature or species concentration) to take a particular value is independent of the spatial position within the reactor [33]. The model resolves, as a function of time, the development of the joint PDF describes the state of the reactor but not as a function of space. This becomes a computationally efficient method that maintains a detailed treatment of the chemistry, whilst also providing a trade-off between the resolution of spatial information and the computational time [31]. For more details on the models employed by SRM the reader is referred to [31].

The validation of the employed engine setup and configuration are summarised in Table 1, details established through the previous works by Cordiner et al. [26] and Maurya et al. [35], which describe the experimental setup and test conditions using natural gas and diesel. The reader is referred to these references for further details on the validation of the employed engine model. All the parameters used in the SRM are summarised in Table 2.

Table 1: Engine specifications

Engine parameter	Value/Description
Engine	IVECO 8360.46R
Type	4-Stroke CI
Number of cylinders	6
Stroke	130 mm
Bore	112 mm
Displacement volume	7.8 L
Compression ratio	17.6:1
Maximum power	166 kW @ 2050 RPM
Maximum torque	965 Nm @ 1250 RPM

The SRM software accounts for the effects of spatial inhomogeneities in the combustion chamber, providing results that are more precise than those obtained from other models, both single and multi-zonal. The stochastic particles can interact with the cylinder walls and other particles during turbulent mixing, mimicking the behaviour of real fluid particles [33]. To compute the combustion parameters, the SRM software uses detailed chemical kinetics. The applied NH_3/H_2 detailed chemical mechanism consists of 38 species and 263 reactions and has been validated in combustion chemistry studies [34]. The SRM software accounts for wall heat losses by employing a Woschni heat transfer correlation for the calculation of the heat transfer coefficient.

Table 2: Parameters used in the stochastic reactor model.

Model Parameter	Value/Option
Initial NH_3/H_2 mass (PFI)	105 mg
Initial pressure	1.4 bar
Initial temperature	330 K
Simulation start	-180 CAD aTDC
Simulation end	180 CAD aTDC
Solver relative tolerance	1.0E-05
Solver absolute tolerance	1.0E-10
Sauter Mean Diameter	10 μm
Nozzle number	6
Nozzle diameter	0.16 mm
Heat transfer model	Stochastic
Heat transfer correlation	Woschni
Woschni C1 parameter	2.28
Woschni C2 parameter	0.02
Stochastic heat transfer constant	2000
Heat mass factor	0.05
Piston wall temperature	550 K
Cylinder head surface area ratio	1.2
Turbulence timescale	0.002 s
Turbulence timescale during injection	0.001 s
Turbulence timescale mode	Empirical KE model
Turbulence mixing mode	Hybrid
Turbulence mixing Cφ	2.0

To account for the dynamic effects of direct injection, including variations in pressure and orifice size, the SRM employs empirical correlations and a refined injector model. These components are integral to simulate the influence of key injection parameters on fuel atomisation, spray behaviour, and subsequent fuel-air mixing. By adjusting the multi-dimensional mass density functions for the composition and temperature within the cylinder, the SRM accounts for fuel distribution and mixing efficiency changes. This methodology enables the simulation of the direct injection's impact on the combustion process within the constraint of the mass density function being spatially homogeneous. This constraint, however, is mitigated by the methodological choice to parameterise, calibrate (parameter estimation) and validate (blind-testing) the sub-models based on experimental data to enhance the model's predictive capability.

In this study, the engine parameters were set according to Table 1 in combination with the parameters in Table 2, with a hydrogen fuel mole fraction of 30% (at 750 and 1,250 rpm) and 40% (at 1,750 rpm). The compression ratio was maintained at 17.6:1 and the stroke and bore were set to 130 and 112mm, respectively. The initial intake cylinder pressure and mixture temperature were set to 1.4 bar and 330K, respectively, representing mild boosting and efficient intercooling which also permits a convenient starting point for ignition by the use of peroxide. Note that we have not attempted to match the details of the boosting of the IVECO engine. The simulations were conducted from −180 crank angle degrees after top dead centre (CAD aTDC) to +180 CAD aTDC. The intake fuel quantity was set to 105 mg, resulting in a fuel consumption rate of 7.875 kg/h at 1250 RPM. The global equivalence ratio (φ) varied between 0.44 and 0.5, depending on the H_2/NH_3 ratio. It is noted that H_2O_2 is assumed to always be diluted in water in concentrations equal to 30 vol%, unless otherwise stated. This is an important parameter because H_2O_2 is readily available in the market up to only about 30 % (w/vol and w/w[1], depending on supplier specification) and above that both its availability and operational convenience decrease significantly. Note though that the difference between 30% w/vol and 30% vol% for H_2O_2 is small, i.e., 30% w/vol is roughly 22% vol%.

The injection parameters of the H_2O_2 solution were adjusted with the understanding that the injected H_2O_2 solution should be less than 10% of the NH_3/H_2 mixture volume in the initial mixture. The motivation for this approach is that, in a dual fuel system such as the one proposed here, it is desired to minimize the dependence on the second (high reactivity) fuel and hence limit as much as possible the size of its respective bunker tank. The current proposal also considers that some H_2 will be produced from ammonia cracking. Therefore, we use the initial mass of ammonia as a reference value. Hence, the mass of 105.0mg of NH_3/H_2 fuel per cycle at a H_2 share of 30% vol% corresponds to

[1] "w/vol" stands for "weight/volume" while "w/w" stands for "weight/weight".

100.0 mg of NH_3. This ammonia amount translates to 0.14 mL. In most simulations, the amount of the directly injected solution (H_2O_2 30 vol%) was 5 mg which corresponds to 0.0042 mL, or 3.1% of the main (NH_3/H_2) blend volume per cycle. Note that all shares of the main fuel blend (NH_3/H_2), air and the directly injected H_2O_2/H_2O refer to *volume*, unless otherwise stated. It is also noted that in energy terms, the amount of 5.0 mg of aqueous H_2O_2 (H_2O_2 30% vol%) corresponds to 1.12% of the energy in the 105mg of the initial fuel NH_3/H_2 (0.7/0.3 per mole fraction); 0.028 kJ for aqueous H_2O_2 and 2.49kJ for NH_3/H_2.

Table 3: Mole fraction (X_F), mass fraction (Y_F), lower heating values (LHV), energy and volume of the individual components of the NH_3/H_2 fuel mix and the directly injected H_2O_2/H_2O solution employed at low-medium (750 and 1,250 rpm) and high (1,750 rpm) engine speeds.

	NH_3	**H_2**	**H_2O_2**	**H_2O**	
X_F	0.3	0.7	0.3	0.7	**750 / 1,250 rpm**
Y_F	0.952	0.048	0.447	0.553	
LHV [MJ/kg]	18.8	120	3.12	0	
105 mg NH_3/H_2	99.92 mg	5.08 mg	-	-	
4 mg DI H_2O_2/H_2O	-	-	1.79 mg	2.21 mg	
Energy [kJ]	1.88	0.61	0.0056	0	
Volume [mL]	0.1369	0.2208	0.0012	0.0022	
X_F	0.4	0.6	0.3	0.7	**1,750 rpm**
Y_F	0.927	0.073	0.447	0.553	
LHV [MJ/kg]	18.8	120	3.12	0	
105 mg NH_3/H_2	97.31 mg	7.69 mg	-	-	
4 mg DI H_2O_2/H_2O	-	-	3.58 mg	4.42 mg	
Energy [kJ]	1.83	0.92	0.0112	0	
Volume [mL]	0.1333	0.3345	0.0025	0.0044	

Results

The results are organized into three main sections. In all sections, the analysis focuses on three engine speeds, 750, 1,250 and 1,750 rpm. In the first part, the mass of the directly injected solution varies from 0.1 to 10.0 mg, while maintaining constant all other parameters. In the second section, the share of H_2O_2 in the directly injected solution varies from 10 to 50% vol%. As in the previous section, all other parameters are kept unchanged. The last section aims to shed some light on the effect of different injection strategies on the engine performance, combustion phasing and emissions. As a result, SOI varies from -20 to -4 CAD aTDC for all engine speeds. This exercise is executed for three different injection durations (ID): 1, 4 and 8 CAD. For reference, the individual properties and quantities (i.e., mass fraction, mole fraction, low heating value, energy, mass, volume) associated with NH_3, H_2, H_2O_2 and H_2O used for the different operating conditions are summarised in Table 3.

Directly injected mass analysis

The analysis starts by examining the effect of varying the mass of the directly injected (DI) solution. In all cases the injection duration was 1 CAD, the mass of the initial NH_3/H_2 mixture was 105 mg, the share of H_2O_2 in the directly injected solution was 30 vol%. The hydrogen molar share in the initial solution was maintained at 30 vol% at 750 and 1,250 rpm and 40 vol% at 1,750 rpm. This change of the H_2 share in the initial NH_3/H_2 mixture at 1,750 rpm was deemed necessary because, at lower H_2 shares, the engine misfired for most examined cases of directly injected masses in the range of 0.1-10.0 mg. Finally, the SOI was at -4, -10

and -14 CAD aTDC for 750, 1,250 and 1,750 rpm, respectively. The SOI values were selected by considering two criteria across the range of the examined conditions: (a) avoidance of misfire; (b) avoidance of excessive pressure rise rate (i.e., above 50 bar/ms). Obviously, these criteria vary with the engine speed, which explains the use of different SOI for each individual engine speed. It is reiterated that no optimisation exercise was performed in view of key variables like the developed power, thermal efficiency, and emissions. Hence, the reported values are not likely to be the optimal ones.

Intuitively, the addition of more pilot fuel is expected to favour the promotion of ignition. This is confirmed in Fig. 1 where the time histories of the in-cylinder pressure, temperature, and heat release rate (HRR) are displayed for various cases of directly injected (DI) mass of solution at 750 rpm. Clearly, the incremental increase of the DI mass of solution tends to progressively: (i) advance the ignition of the charge; (ii) increase the maximum pressure, temperature and heat release rate (HRR). Since the ignition with the lowest DI mass of H_2O_2/H_2O mixture occurs after TDC and late in the power stroke, any advance in SOI will tend to bring the ignition closer to the TDC where the pressure is higher. As a result, the thermodynamic conditions are more favorable for ignition, thereby leading not only to an earlier ignition but also to higher maximum pressure, temperature, and heat release rate. It is worth making some further observations. The increase of the DI mass of solution from 2.0 to 5.0 and 10.0 mg corresponds to an increase of only 0.17% and 0.45% in the total fuel heating value (considering an LHV of 23.5 J/mg for the NH_3/H_2 70/30 vol% mixture and 1.39 J/mg for the H_2O_2/H_2O 30/70 vol% mixture, an initial mass of 105.0 mg for the NH_3/H_2 mixture and 2.0 mg for the DI H_2O_2/H_2O mixture, resulting in a total heating value of $105\ mg \times 23.5 \frac{J}{mg} + 2\ mg\ \times 1.39 \frac{J}{mg} = 2470\ J$). This negligible increase is to be expected because the lower heating value (LHV) of the DI solution is only 5.9% of that of the main fuel, *i.e.*, NH_3/H_2, and the fraction of the DI solution relative to the NH_3/H_2 mixture never exceeds 1/10th on a mass basis, even when injecting 10.0 mg of solution. Hence, it is not surprising that the cumulative heat release exhibits an increase of 0.29% and 0.69% for the cases of 5.0 and 10.0 mg of DI mass of solution, respectively, compared to the case of 2 mg. However, the *effect* of the increase of the DI mass of solution becomes more pronounced in view of the maximum pressure; the increase from 2.0 to 5.0mg, and subsequently to 10.0 mg leads to a maximum pressure increase of 22.1% and 37.05%, respectively. This spectacular increase is the outcome of the combustion phasing during which the radical pool enhancement is favored. An unambiguous manifestation of this radical pool enhancement is the fact that the maximum mass fraction of OH increases by 47% and 63% when the mass of the DI solution increases from 2.0 to 5.0 mg, and to 10.0 mg, respectively (maximum mass fraction of OH: 1.79E-04, 2.63E-04, 2.91E-04 for the cases of 2.0, 5.0 and 10.0 mg, respectively). The reader should also recall that the dissociation reaction $H_2O_2(+M) \rightarrow 2OH(+M)$, which is the main facilitator for the radical pool enhancement due to the introduction of H_2O_2, is an endothermic and not an exothermic one. As the radical pool increases due to the introduction of H_2O_2, the temperature increase is limited by: (i) the cooling effect that occurs because of the solution evaporation; (ii) the introduction of H_2O which acts as diluent; (iii) reaction $H_2O_2(+M) \rightarrow 2OH(+M)$ that accelerates the generation of OH radicals. However, the increase of the DI mass of solution comes with the caveat of a more pronounced cooling effect. This is illustrated in the inset of the temperature history graph, where it is shown that the temperature *decreases* with the increase of the DI mass of H_2O_2/H_2O, but it soon picks up before the steep increase due to chemical reaction.

Having obtained some insight on the effect of the increase of the DI mass of solution on the engine heat release rate, attention was shifted to the effects on engine performance, combustion phasing and NO_x emissions. This is illustrated concisely in Fig. 2, where the effect of the DI mass of solution on indicated torque, indicated thermal efficiency (n_{th}), CAD50, combustion duration (represented by CAD90-CAD10), maximum pressure rise rate and specific NO_x are shown for engine speeds of 750, 1,250 and 1,750 rpm. It is noted that CAD50 represents the crank angle location for 50% heat release while CAD90-CAD10 denotes the crank angle duration from 10% to 90% of the heat release. At 750 rpm, the minimum required mass of DI H_2O_2/H_2O solution to avoid misfire was 2 mg while at 1,250 and 1,750 rpm that minimum quantity increased to 3 mg.

Starting with the effect on the indicated torque, 2.0 mg of DI solution at 750 rpm leads to 627 Nm (for the purposes of comparison, this corresponds to 65% of the maximum rated torque of 965 Nm when using diesel fuel at 1250 rpm. Note earlier comments about the disparity in the levels of boost between this simulation and the operation of the engine on diesel fuel). At 1,250 rpm, the *minimum* required quantity of DI solution is 3.0 mg, leading to 658 Nm (*i.e.*, 68% of the maximum rated torque at the same engine speed).

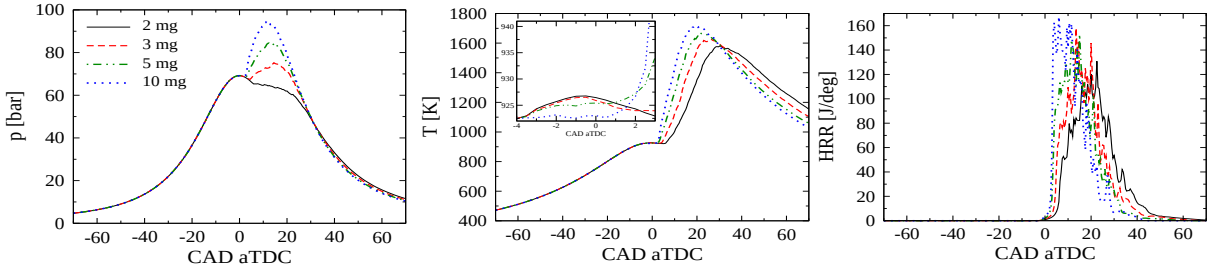

Fig. 1. The time history of pressure (left), temperature (middle) and heat release rate (right) for four cases of directly injected mass of H_2O_2/H_2O (2, 3, 5 and 10 mg) with the SOI fixed at -4 CAD aTDC. The hydrogen share was kept at 30% (750 and 1,250 rpm) and 40% (1,750 rpm) vol%, the injection duration was 1 CAD, the mass of the initial NH_3/H_2 mixture was 105.0 mg, the share of H_2O_2 in the directly injected diluted mixture was 30% vol% and the engine speed was 750 rpm.

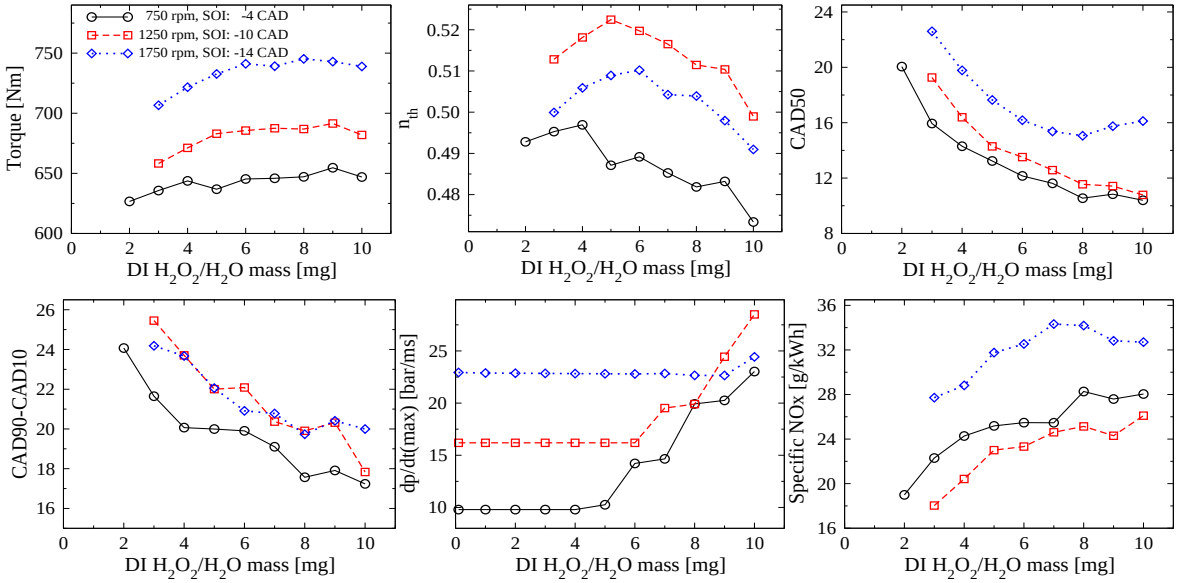

Fig. 2. The change in indicated torque, indicated thermal efficiency (n_{th}), CAD50, CAD90-CAD10, maximum pressure rise rate and specific NO_x as a function of the directly injected (DI) mass of H_2O_2/H_2O (0.1-1 mg), for three engine speeds: 750, 1,250 and 1,750 rpm. The SOI was maintained constant at -4, -10 and -14 CAD aTDC for 750, 1,250 and 1,750 rpm, respectively. The hydrogen share was maintained at 30% at 750 and 1,250 rpm and 40% in the case of 1,750 rpm. In all cases, the injection duration was 1 CAD, the mass of the initial NH_3/H_2 mixture was 105.0 mg, and the share of H_2O_2 in the directly injected diluted mixture was 30%.

Finally, at 1,750 rpm, 3.0 mg of DI solution achieves an indicated torque 73% of the maximum rated at 1250 rpm. Figure 2 shows that the progressive *increase* of the mass of the DI solution beyond the values in the preceding sentences initially leads to notable increase of the indicated torque before levelling off at all engine speeds. Hence, the maximum indicated torques of 655 Nm, 691 Nm and 745 Nm are achieved at engine speeds of 750, 1,250 and 1,750 rpm, respectively. These values correspond to 4.5%, 5.1% and 5.5% increases (for 750, 1,250 and 1,750 rpm, respectively) compared to their respective minimum values obtained for 2.0 and 3.0 mg of solution. After reaching its maximum value (9.0 mg at 750 rpm, 1,250 rpm and 8.0 mg at 1,750 rpm), the indicated torque exhibits some negligible decrease. As has already been shown in Fig. 1, and will further be supported in Fig. 2, the incremental increase of the mass of the DI solution leads to ignition advance and increase of the maximum pressure which, combined, lead to higher indicated work and indicated torque.

The indicated torque results for 750 and 1,250 rpm need some explanation, given that the energy

input is the same (i.e., the NH_3 and H_2 shares are the same). As the engine speed increases, Fig. 2 shows that at the same DI H_2O2/H_2O mass, the indicated torque increases. This seems counterintuitive because, by increasing the engine speed, the time per stroke decreases and hence there is less time available for the fuel to fully react. However, note that when the engine speed increases from 750 to 1,250 rpm, the SOI was also advanced from –4 to –10 CAD aTDC. The balance between these two times (the time per stroke and the SOI) results in the emission of smaller amounts of unburnt ammonia for the case of 1,250 rpm and hence a higher cumulative heat release (especially later in the power stroke) which increases the produced torque. This is consistent with the difference in the thermal efficiencies shown in the figure, with that at the higher speed being the greatest. Similar arguments hold for Figs. 5 and 8 that will be discussed next.

The effect of the increase in the DI mass of solution on the indicated thermal efficiency is qualitatively similar to the one previously described for the indicated torque, i.e., it gradually reaches a local maximum value. This is not surprising as indicated thermal efficiency largely depends on the indicated power. The fuel mass flow rate ($\dot{m}_f$), the other component in the calculation of the indicated thermal efficiency, increases linearly with the increase of the DI mass of solution while the fuel heating value (LHV) is constant. Figure 2 also shows that the maximum thermal efficiency is reached for the following values of DI mass of solution: 4.0 mg at 750 rpm ($n_{th} = 0.497$), 5.0 mg at 1,250 rpm ($n_{th} = 0.522$), and 6.0 mg at 1,750 rpm ($n_{th} = 0.51$). The notable decrease that the indicated thermal efficiency exhibits as a function of the DI mass of H_2O_2/H_2O is a result of the variation in the local maximum value of power while the mass flow rate increases monotonically.

The effect of the DI mass of solution on combustion phasing is initially quite pronounced with the increase of the DI mass. Compared to the minimum required DI mass of 2.0 or 3.0 mg of solution[2], CAD50 advanced to 10.4 CAD (48% decrease) at 750 rpm (10.0 mg), 10.8 CAD (44% decrease) at 1,250 rpm (10.0 mg) and 15.1 CAD (33% decrease) at 1,750 rpm (8.0 mg). However, the greatest influence of the DI mass of solution occurs at low mass values and this diminishing effect of the DI mass on CAD50 also partly explains its decreasing effect on indicated torque (noted earlier). Here, it is interesting to note that the direct injection of H_2O_2/H_2O solution occurs, in all cases, relatively far from the TDC: -4, -10 and -14 CAD aTDC for 750, 1,250 and 1,750 rpm, respectively, and is completed after only 1 CAD of injection. So, the question that naturally rises is: why does the effect on CAD50 of the increase of the DI mass become increasingly attenuated, despite the fact that the end of injection is completed relatively far (advanced) from TDC? A possible explanation for this phenomenon is that the increase of directly injected mass is accompanied by the increase of not only H_2O_2 but also of H_2O, with the latter being the dominant component in the mixture. So, although the increase of H_2O_2 favors the promotion of ignition, the increase of H_2O has an opposite effect. When the mass of the DI H_2O_2/H_2O mixture is small, so is that of the mass of H_2O, and hence the effect of the diluent (H_2O) is negligible. By increasing the mass of the DI solution, the mass of H_2O increases and so does its ability to dilute the mixture. In addition, the enthalpy of evaporation of H_2O is much larger than that of H_2O_2, as will also be discussed next.

The combustion duration (CAD90-CAD10) follows a trend similar to CAD50, i.e., its initial decrease is rapid with the increase of the DI mass of solution. At 750 rpm the combustion duration varies between 24.1 CAD (2 mg H_2O_2/H_2O) and 17.2 CAD (10.0 mg H_2O_2/H_2O), which is equivalent to a 28.4% decrease. At 1,250 rpm the variation of the combustion duration is similar, between 25.5 CAD (3.0 mg) and 17.8 CAD (10.0 mg), while at the higher engine speed of 1,750 rpm the variation is smaller still, between 24.2 CAD (3.0 mg) and 19.7 CAD (8.0 mg).

The picture that emerges from the examination of CAD50 and combustion duration is consistent in principle with the findings reported earlier in Fig. 1: increasing the mass of the DI solution enhances the ignition promotion, in that ignition is not only advanced in the power stroke but also has shorter duration. These findings imply that that the maximum pressure rise rate inevitably increases with the mass of the DI solution. This is indeed the case as Fig. 2 illustrates, where it is shown that although for low DI mass values the maximum pressure rise rate is constant, eventually it starts increasing at all engine speeds. The highest

[2] depending on the engine speed, 2 mg for 750 rpm and 3 mg for 1,250 and 1,750 rpm

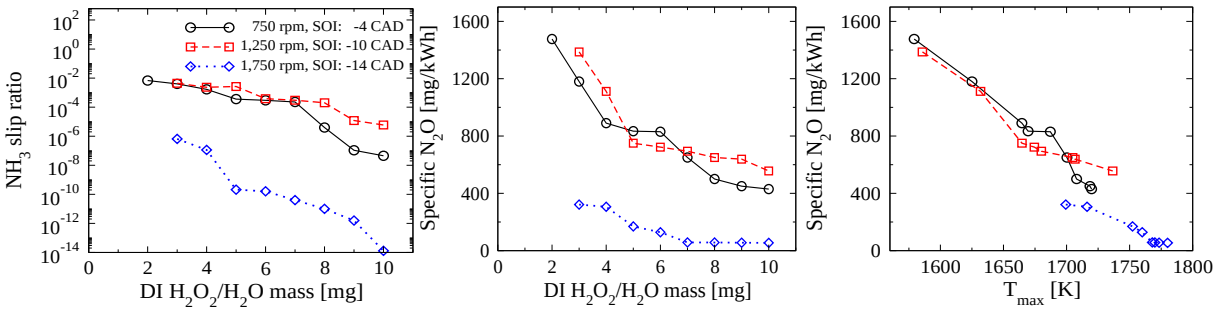

Fig. 3. The change in NH_3 slip ratio and specific N_2O as a function of the directly injected (DI) mass of H_2O_2/H_2O (0.1-1 mg) and maximum temperature, for three engine speeds: 750, 1,250 and 1,750 rpm. The SOI was maintained constant at -4, -10 and -14 CAD aTDC for 750, 1,250 and 1,750 rpm, respectively. The hydrogen share was maintained at 30% at 750 and 1,250 rpm and 40% in the case of 1,750 rpm. In all cases, the injection duration was 1 CAD, the mass of the initial NH_3/H_2 mixture was 105 mg, the share of H_2O_2 in the directly injected diluted mixture was 30%.

percentage increase of the maximum pressure rise rate is observed in the case of 750 rpm, reaching the value of 23 bar/ms (10.0 mg DI H_2O_2/H_2O), equivalent to 135.1% increase compared to the initial value of 9.8 bar/ms with 2.0 mg DI H_2O_2/H_2O. At 1,250 rpm the maximum pressure rise rate reached is 28.5 bar/ms (10.0 mg DI H_2O_2/H_2O), corresponding to an increase of 76% compared to the initial value of 16.2 bar/ms with 3.0 mg DI H_2O_2/H_2O. At 1,750 rpm the increase of the maximum pressure rise rate is markedly more limited, reaching a maximum value of 24.4 bar/ms with 10.0 mg of DI H_2O_2/H_2O, which corresponds to a 7% increase compared to the initial value of 22.8 bar/ms (3.0 mg DI H_2O_2/H_2O). Since the maximum pressure rise is inherently related to the ignition timing (CAD50) and the combustion duration (CAD90-CAD10), it is then natural that the effect of the DI H_2O_2/H_2O mass increase is stronger at lower engine speeds where the ignition timing was closer to the TDC, and the combustion duration was shorter. Notice, however, that the maximum values reached at all engine speeds - despite their significant increase - are still far below the value of 50 bar/ms that is commonly accepted as the threshold for normal engine operation.

Specific NO_x emissions are primarily a function of the maximum temperature reached. Figure 1 shows that the increase of the DI mass of solution leads to an increase of the maximum temperature. This behavior is consistent at all engine speeds. It is then reasonable to expect that NO_x emissions also, in principle, increase with the DI mass of solution. The range of NO_x emissions reached for DI mass of solution ranging between 2.0 and 10.0 mg is 19 – 28 kWh, 18 – 26.1 g/kWh and 27.7 – 34.3 g/kWh, at 750, 1,250 and 1,750 rpm, respectively. In addition, for the same amount of DI H_2O_2/H_2O mass: (i) NO_x emissions drop when increasing the engine speed from 750 to 1,250 rpm; (ii) NO_x emissions increase when increasing the engine speed from 750 to 1,750 rpm. At first glance, this non-monotonic response of the NO_x emissions as a function of the engine speed appears counterintuitive. When increasing the engine speed from 750 to 1,250 rpm, the DI mass of H_2O_2/H_2O and the initial NH_3/H_2 mix are kept unchanged. The higher engine speed means that the charge has less time to fully combust which leads to slightly reduced combustion temperatures, with a temperature reduction ranging between 5 and 40 K, thereby leading to lower NO_x emissions. On the other hand, when the engine speed increases from 750 to 1,250 rpm, although the DI mass of H_2O_2/H_2O and the initial NH_3/H_2 mass are both kept unchanged, the hydrogen share in the NH_3/H_2 mix increases by 10%. That increase plays a key role in enabling a fast and complete combustion of the charge with a richer radical pool, thereby leading to higher temperatures and consequently to higher NO_x emissions, as observed in Fig. 2. It is recalled that the IMO's Tier III standard regulates NO_x emissions based on the engine speed, $9 \times n^{-0.2}$, where n the engine speed is in rpm. Hence, at 750, 1,250 and 1,750 rpm, the NO_x standards become 2.39, 2.16 and 2.02 g/kWh, respectively. The minimum NO_x values previously reported while varying the mass of DI solution are thus roughly an order of magnitude higher than the IMO'S Tier III standards. Therefore, either an aftertreatment mechanism should be in place, or some NO_x control strategy should be explored, such as the use of EGR.

Ammonia slip is another challenge related to the use of NH_3 as main fuel in internal combustion engines: it refers to the amount of unburnt ammonia that reaches the exhaust. In the current study, the quantitative analysis of ammonia slip employed the ammonia slip ratio, defined as the amount of NH_3 at the exhaust over the initial amount of NH_3 at the start of the engine cycle. For reference, the initial amount of NH_3 was 99.931 mg and 97.320 mg for the cases of 750/1,250 rpm and 1,750 rpm, respectively. As is illustrated in Fig. 3, for the examined cases the NH_3 slip ratio never exceeds 0.7% and a clear monotonic trend as a function of the amount of the directly injected H_2O_2/H_2O mixture is demonstrated at all engine speeds. This decreasing trend is due to the more intense, hence more complete, combustion process that was also demonstrated earlier in Fig. 2. In addition, Fig. 3 shows that the lowest NH_3 slip ratio values are obtained in the case of 1,750 rpm. Specifically, in the cases of 750 and 1,250 rpm the NH_3 slip ratio varies between 0.7% and 0.0000045%. In absolute mass numbers these ratios translate to a variation between 0.68 mg and $4.5 \cdot 10^{-6}$ mg. At 1,750 rpm the NH_3 slip ratio reaches much lower values, namely a variation between $2.5 \cdot 10^{-5}$ % and $1.3 \cdot 10^{-12}$ %. It is believed that the much lower NH_3 slip ratio values achieved in the case of 1,750 rpm are due to the higher H_2 share in the NH_3/H_2 mix (40% in the case of 1,750 rpm, whereas 30% at 750 and 1,250 rpm) which allows for a more complete combustion of the fuel blend. It is highlighted that the NH_3 slip ratio values reported in Fig. 3 are significantly below other studies reported in the literature that used ammonia as main fuel in a compression ignition engine mode, e.g., [36-38].

Unlike NO_x emissions which are clearly regulated by the IMO, N_2O emissions are not currently regulated by any international organisation. However, N_2O is a very potent greenhouse gas (GHG), therefore it needs to be monitored. In the current study, specific N_2O emissions are reported in Fig. 3, i.e., N_2O mass (mg) emitted scaled by the energy (kWh) produced at the current engine cycle. Firstly, it can be observed that N_2O emissions are higher at 750 and 1,250 rpm than 1,750 rpm. This can be explained by the higher NH_3 share at these lower engine speeds, consistent with what has been reported in the literature [39]. Secondly, there is a clear decreasing trend of the N_2O emissions as a function of the directly injected mass, regardless the engine speed. To explain this trend, we need to consider that N_2O emissions are largely affected by temperature, tending to increase as the temperature drops, as the chemical pathways related to its formation are favored at relatively low temperatures [40]. In the right panel in Fig. 3 the maximum temperature of each case has been plotted against the specific N_2O emissions, for all engine speeds. It is clearly demonstrated that specific N_2O emissions are negatively correlated with the maximum temperature, as expected. The N_2O emissions reported in Fig. 3 are relatively high, varying between 1,477 and 430 mg/kWh at 750 rpm, 1,387 and 556 mg/kWh at 1,250 rpm, and between 321 and 54 mg/kWh at 1,750 rpm. These values are consistent with other studies in the literature that used ammonia as main fuel, e.g., [36, 39, 41-43].

Hydrogen peroxide mixture concentration analysis

In the next part of the analysis, the focus shifts to the share of H_2O_2 in the DI solution. To accomplish a meaningful comparison, all other parameters were kept unchanged: (i) the injection duration was 1 CAD; (ii) the mass of the initial NH_3/H_2 mixture was 105.0 mg; (iii) the hydrogen share in the initial NH_3/H_2 mixture was maintained at 30 vol% at 750 and 1,250 rpm and 40 vol% in the case of 1,750 rpm; (iv) the mass of the DI solution was 5.0 mg at 750 and 1,250 rpm and 10.0 mg at 1,750 rpm; (v) the SOI was at -4, -10 and -14 CAD aTDC for 750, 1,250 and 1,750 rpm, respectively. By increasing the H_2O_2 share in the DI solution, the energy density of the solution increases. Table 4 summarises the variation in the density, the standard enthalpy of evaporation and the energy density as a function of the H_2O_2 share in the solution. The key findings from Table 4 are the following: (i) the increase of the H_2O_2 share increases the mixture's energy density thereby enhancing the combustion process, but that energy density is generally quite poor especially when compared with more conventional fuels like diesel (45.6 MJ/kg); (ii) the standard enthalpy of evaporation of H_2O_2 is quite high when compared with more conventional fuels (for comparison, diesel's is 0.332 MJ/kg) and this will have an adverse effect on the combustion process as it will tend to make more pronounced the cooling effect during the direct injection of the mixture. Another important message that Table 4 conveys is that although on a *mass* basis 5.0 mg of DI H_2O_2/H_2O mixture represents 4.8% of the NH_3/H_2 initial mass (105.0 mg), on an *energy* basis this ratio is significantly lower and ranges between 0 (0% H_2O_2) and 0.63% (100% H_2O_2) depending the H_2O_2 share in the solution (taking an LHV of 23.5 MJ/kg for the NH_3/H_2 mixture). This is simply the result of the much higher LHV that the NH_3/H_2 mixture possesses.

Table 4: The variation of selected properties due to the change of the H_2O_2 share in the DI H_2O_2/H_2O mixture.

% H_2O_2 vol%	% H_2O_2 /mass	Density [kg/m³]	Standard enthalpy of evaporation [MJ/kg]	LHV [MJ/kg]	Heating value of 5 mg H_2O_2/H_2O [J]
0	0	997	2.308	0	0
10	17	1076	2.154	0.54	2.70
20	32	1142	2.023	0.99	4.99
30	45	1120	1.911	1.39	6.97
40	56	1249	1.813	1.74	8.68
50	65	1293	1.727	2.04	10.18
100	100	1450	1.42	3.12	15.60

In principle, increasing the H_2O_2 share in the DI solution can have a positive effect on the combustion process. This is illustrated in Fig. 4 where it is shown that the progressive increase of the H_2O_2 share from 20% to 40% leads to a significant ignition advance and higher pressures. The ignition promotion is also manifested in the temperature history which increases with the H_2O_2 share [3]. In Fig. 4 it is shown that the increase of the H_2O_2 share leads to a substantial enhancement of the radical pool, as manifested in the time histories of the molar concentrations of OH and H radicals. Most important is that this radical pool enhancement occurs right after the completion of injection, as the insets to the OH and H graphs illustrate. To add some perspective, at -7 CAD aTDC the temperature in the case of 30% H_2O_2 share in the DI solution is 910.7 K, i.e., barely 0.8 K up from the case of 20% H_2O_2 share at the same CAD (909.9 K), or in other words, 0.09% increase. On the other hand, the molar concentrations of OH and H exhibit 44% and 35% increases, respectively, in their values at the same instants for the same H_2O_2 share comparison cases.

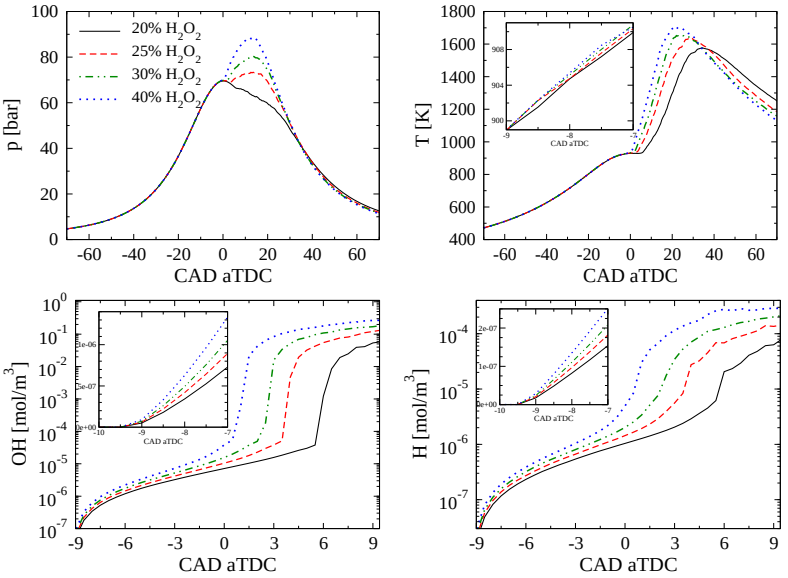

Fig. 4. The time history of pressure, temperature, and the molar concentrations of OH and H radicals for four cases of directly injected mass of H_2O_2/H_2O mixture, with the share of H_2O_2 in the directly injected diluted mixture varying between 20% and 40%. In all cases, the hydrogen share was kept at 30%, the injection duration was 1 CAD, the SOI was maintained at -10 CAD aTDC, the mass of the initial NH_3/H_2 mixture was 105.0 mg, the mass of the directly injected H_2O_2/H_2O mixture was 5.0 mg and the engine speed was 1,250 rpm.

All these findings corroborate further the physical mechanism that enables the H_2O_2/H_2O mixture to act as an effective ignition promoter, namely by primarily enhancing the radical pool generation.

[3] The inset in the temperature figure also highlights that as the H_2O_2 share increases, the temperature increases slightly faster in the early phase just after the completion of the direct injection of the H_2O_2/H_2O mixture, a phenomenon which can be attributed to the decreased cooling effect of the directly injected mixture. This occurs owing to the decrease of the standard enthalpy of evaporation achieved by the increase of the H_2O_2 share, as was also highlighted in Table 4. However, this diminishing cooling effect is barely visible and although it favors the overall combustion process, the main reason for the ignition promotion is the radical pool enhancement, an argument that was also raised in the previous section.

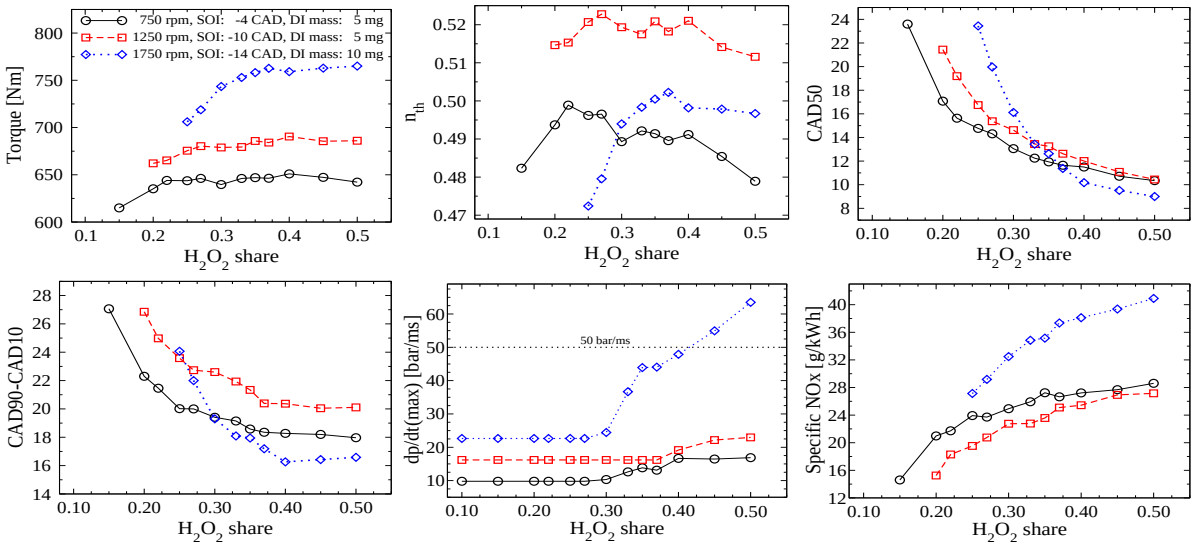

Fig. 5. The change in indicated torque, indicated thermal efficiency (n_{th}), CAD50, CAD90-CAD10, maximum pressure rise rate and specific NO_x as a function of the H_2O_2 share in the directly injected (DI) mass of H_2O_2/H_2O mixture, for three engine speeds: 750, 1,250 and 1,750 rpm. The SOI and DI mass of H_2O_2/H_2O mixture were maintained constant at -4 CAD aTDC/5 mg, -10 CAD aTDC/5 mg and -14 CAD aTDC/10 mg for 750, 1,250 and 1,750 rpm, respectively. The hydrogen share was maintained at 30% at 750 and 1,250 rpm and 40% in the case of 1,750 rpm. In all cases, the injection duration was 1 CAD and the mass of the initial NH_3/H_2 mixture was 105 mg.

The analysis is then extended to include engine speeds from 750 up to 1,750 rpm, as displayed in Fig. 5, which explores the effect of the H_2O_2 share on the indicated torque, the indicated thermal efficiency, CAD50, the combustion duration (CAD90-CAD10), the maximum pressure rise rate and the specific NO_x emissions, for H_2O_2 shares ranging between 15% up to 50%. The reader is reminded that the H_2O_2 share refers to the DI solution and the mass of the latter is maintained constant at 5.0 mg at 750 and 1,250 rpm and at 10.0 mg at 1,750 rpm, while the mass of the initial NH_3/H_2 fuel is kept unchanged for all cases at 105.0 mg.

Starting with the effect on the indicated torque, Fig. 5 shows that the increase of the H_2O_2 share has in principle a positive effect, regardless of the engine speed. At all three examined speeds, the progressive increase of the H_2O_2 share in the DI solution leads to initially a relatively rapid increase of the indicated torque. Hence, the maximum torque values are obtained for 40% H_2O_2 share at 750 and 1,250 rpm (651 and 691 Nm, respectively) and 50% H_2O_2 share at 1,750 rpm (765 Nm). The torque developed with an H_2O_2 share of 30% at all engine speeds is extremely close to the aforementioned maximum values: barely -1.7% at 750 and 1,250 rpm and -2.8% at 1,750 rpm. This is an important finding because it suggests that solutions with 30% H_2O_2 share (readily commercially available) can result in the development of a torque close to the maximum possible. H_2O_2/H_2O mixtures with lower H_2O_2 shares could also possibly work quite effectively but not for higher speeds (not shown here). For example, an H_2O_2/H_2O mixture with 20% H_2O_2 share enables the production of 635 Nm and 662 Nm at 750 and 1,250 rpm, respectively, which are merely -2.4% and -4.1% lower than their respective maximum values.

The indicated thermal efficiency exhibits a slightly different response compared to torque, as it produces a local maximum. This is an expected response if we recall that thermal efficiency is the ratio of power over the product of the fuel mass flow rate and the overall fuel heating value. The mass flow rate is maintained constant as the H_2O_2 share increases, but the overall fuel heating value increases linearly. Therefore, the denominator in the definition of the thermal efficiency increases linearly with the increase of the H_2O_2 share. At the same time, the power (following the same response as torque) has a weak local maximum resulting in the variation in the figure. In terms of the indicated thermal efficiency, Fig. 5 shows that maximum values of 0.499 (750 rpm, 22% H_2O_2 share), 0.523 (1,250 rpm, 27% H_2O_2 share) and 0.502 (1,750 rpm,

37% H_2O_2 share) are obtained. With 30% H_2O_2 share in the DI solution, the indicated thermal efficiency is 0.489, 0.519 and 0.494 at 750, 1,250 and 1,750 rpm, respectively. These values are -2.58%, -0.86% and -1.05% lower compared to the maximum ones, thereby suggesting that the use of a solution with 30% H_2O_2 share would suffice to achieve optimal operational efficiency.

The ignition advance achieved with the increase of the H_2O_2 share in the DI solution is reflected in the value of CAD50, as shown in Fig. 5. The effect of the H_2O_2 share increase is stronger at relatively low H_2O_2 shares. As already argued, the main reason for the ignition advance induced by H_2O_2 stems from its ability to enhance the radical pool. This was evidenced previously by examining the time history of important radicals like OH and H. Here, this argument is strengthened further. Figure 6 displays the variation of CAD50 as a function of the maximum molar concentration of OH for the same cases examined in Fig. 4, at all three engine speeds. It is evident that CAD50 advances in an almost perfectly linear manner with the maximum OH. In fact, by performing a linear regression analysis, the coefficient of determination value (R^2) is found to be ~0.97 for all three engine speeds. Another interesting finding is that the regression analysis on the results obtained for 750 and 1,250 rpm reveals that the obtained fitted regression lines are almost identical between these two engine speeds, exhibiting only negligible differences. The case of 1,750 rpm exhibits a different regression line but this is expected as the DI mass of the solution is 10.0 mg (instead of 5.0 mg at the other two engine speeds).

The ignition advance achieved with the increase of the H_2O_2 share in the H_2O_2/H_2O mixture is accompanied by shorter combustion duration. Figure 5 shows that CAD90-CAD10 decreases steadily for all engine speeds with the increase of the H_2O_2 share in the solution. By increasing the H_2O_2 share from 15% to 25% at 750 rpm the combustion duration drops by 26%. This is a truly remarkable impact considering that 15% of H_2O_2 share in a 5.0 mg H_2O_2/H_2O mixture corresponds to 1.25 mg of H_2O_2 while, when the H_2O_2 share is increased to 25%, the mass of H_2O_2 becomes 1.93 mg. So, the 26% decrease of the combustion duration is in fact owing to an increase of only 0.68 mg of H_2O_2. In a similar fashion at the higher speed, *i.e.* at 1,250 rpm, increasing the H_2O_2 share from 20% to 30% results in 15% decrease of duration, while at the highest engine speed, *i.e.* at 1,750 rpm, a 10% increase of the H_2O_2 share from 25% to 35% results in 25.4% decrease of the combustion duration. All these results corroborate the strong effect of H_2O_2 in expediting the combustion process.

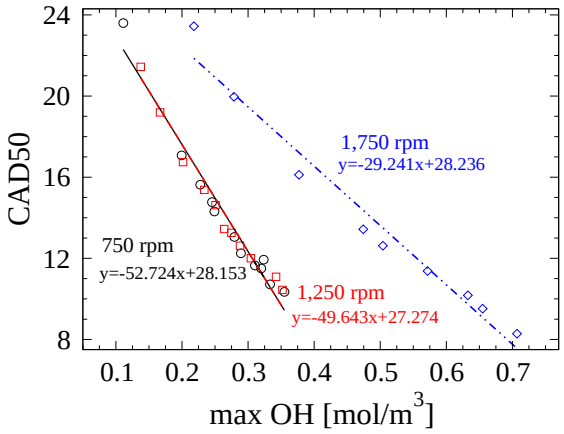

Fig. 6. The change of CAD50 as a function of the maximum molar concentration, by varying the H_2O_2 share in the directly injected (DI) mass of H_2O_2/H_2O mixture, for engine speeds of 750, 1,250 and 1,750 rpm. The SOI and DI mass of H_2O_2/H_2O mixture were maintained constant at -4 CAD aTDC/5.0 mg, -10 CAD aTDC/5.0 mg and -14 CAD aTDC/10.0 mg for 750, 1,250 and 1,750 rpm, respectively. The H_2 share was maintained at 30% at 750 and 1,250 rpm and 40% in the case of 1,750 rpm. In all cases, the injection duration was 1 CAD and the mass of the initial NH_3/H_2 mixture was 105/0 mg.

The shortening of the combustion duration, and the advance of CAD50, because of the increase of the H_2O_2 share in the solution is expected to result in a more intense combustion, manifested by the maximum pressure rise rate. This expectation is confirmed in Fig. 5. However, this occurs for relatively high H_2O_2 shares only. A 30% H_2O_2 share results in 10.3, 16.2 and 24.4 bar/ms at 750, 1,250 and 1,750 rpm, respectively. All these values are well below the threshold of 50 bar/ms for normal and safe engine operation. In fact, at most examined conditions, the maximum pressure rise rate does not exceed 28.5 bar/ms. However, Fig. 5 also shows that for sufficiently high H_2O_2 shares, the maximum pressure rise rate can in fact increase significantly, even above the threshold of 50 bar/ms. This only occurs for the highest engine speed (1,750 rpm) and not the lower ones. Increasing the H_2O_2 share above 30% results in a steep increase of the maximum pressure rise rate, approaching close to the threshold of 50 bar/ms with a 35% H_2O_2 share, and exceeding it with a 45% H_2O_2 share. The different response that is observed in the case of 1,750 rpm compared to the other two engine speeds can be attributed to the higher mass of the directly injected solution (double

that used at the lower engine speeds). Although a 30% share appears to be a safe option for normal engine operation at all examined engine speeds, these results warn of a risk of excessive pressure rise rate if the H_2O_2 share is not wisely selected.

The last subfigure in Fig. 5 concerns the variation of specific NO_x as a function of the H_2O_2 share in the solution. NO_x emissions progressively increase with the increase of the H_2O_2 share at all engine speeds. However, this trend becomes less pronounced with the increase of the H_2O_2 share and tends to level off. For example, an increase of the H_2O_2 share from 20% to 30% at 750 rpm results in a 18.8% rise of NO_x emissions but further increase from 30% to 40% results in 9.2% rise and finally going from 40% to 50% H_2O_2 share leads to a respective increase of 5.1% in NO_x emissions. In any case, NO_x emissions are inherently coupled with the combustion temperature, hence, it is natural to expect some correlation between the maximum temperature and the NO_x emissions. Figure 7 confirms a closely linear correlation in the variation of specific NO_x against the maximum temperature for all the cases of H_2O_2 share increase displayed in Fig. 5. The regression analysis reveals a linear correlation at all engine speeds, with the coefficient of determination value (R^2) being 0.99, 0.97 and 0.99 for the three engine speeds. Most important, the slopes of all three regression lines are nearly identical, thereby corroborating the strong and linear dependence of NO_x emissions to the maximum temperature. In terms of the actual values of specific NO_x that are attained with the various H_2O_2 shares, these range between 14.6 and 28.6 g/kWh at 750 and 1,250 rpm and between 27.1 and 40.9 g/kWh at 1,750 rpm. The much higher NO_x values reached in the case of 1,750 rpm are due to the significantly greater DI mass of solution (double that used at the lower engine speeds). With a 30% H_2O_2 share in the solution, the specific NO_x values are 24.9 (750 rpm), 22.8 (1,250 rpm) and 32.5 g/kWh (1,750 rpm), thereby exceeding the IMO's Tier III standards by an order of magnitude (2.39, 2.16 and 2.02 g/kWh for engine speeds of 750, 1,250 and 1,750 rpm, respectively).

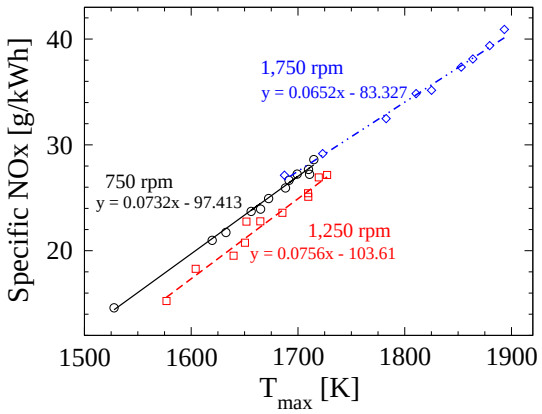

Fig. 8. The change of specific NO_x as a function of the maximum temperature, by varying the H_2O_2 share in the directly injected (DI) mass of H_2O_2/H_2O mixture, for engine speeds of 750, 1,250 and 1,750 rpm. The SOI and DI mass of H_2O_2/H_2O mixture were maintained constant at -4 CAD aTDC/5 mg, -10 CAD aTDC/5 mg and -14 CAD aTDC/10 mg for 750, 1,250 and 1,750 rpm, respectively. The H_2 share was maintained at 30% at 750 and 1,250 rpm and 40% in the case of 1,750 rpm. In all cases, the injection duration was 1 CAD and the mass of the initial NH_3/H_2 mixture was 105.0 mg.

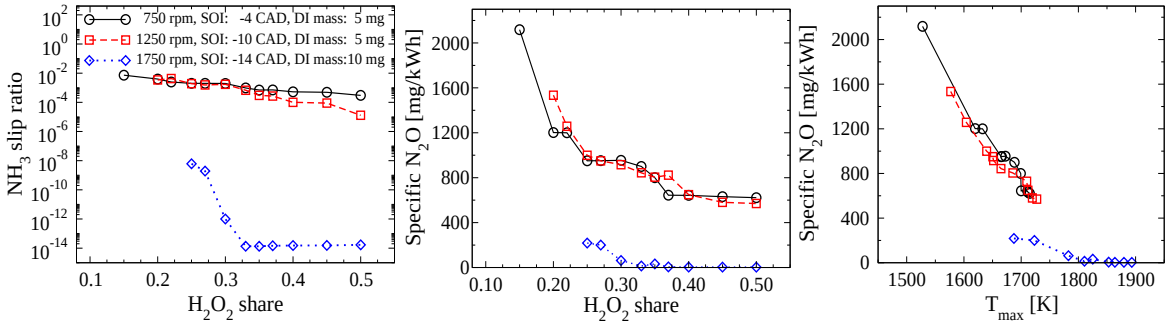

Fig. 7*:* The change in NH_3 slip ratio and specific N_2O as functions of the H_2O_2 share in the directly injected (DI) mass of the H_2O_2/H_2O mixture and of the maximum temperature, for three engine speeds: 750, 1,250 and 1,750 rpm. The SOI and DI mass of H_2O_2/H_2O mixture were maintained constant at -4 CAD aTDC/5.0 mg, -10 CAD aTDC/5.0 mg and -14 CAD aTDC/10.0 mg for 750, 1,250 and 1,750 rpm, respectively. The hydrogen share was maintained at 30% at 750 and 1,250 rpm and 40% in the case of 1,750 rpm. In all cases, the injection duration was 1 CAD and the mass of the initial NH_3/H_2 mixture was 105.0 mg.

The ammonia slip ratio is illustrated in Fig. 8 along with the specific N_2O emissions, both as a function of the H_2O_2 share in the directly injected mixture. The initial mass of ammonia in the NH_3/H_2 mix is 99.9 mg for the engine speeds of 750 and 1,250 rpm and 97.3 mg at 1,750 rpm. The figure shows that the unburned ammonia is extremely low in all examined cases, and it is negatively correlated with the H_2O_2 share in the directly injected solution. Specifically, the NH_3 slip ratio varies between 0.73% (0.725 mg) and 0.03% (0.03 mg) at 750 rpm, between 0.3% (0.34) and 0.001% (0.001 mg) at 1,250 rpm, and between $5.9 \cdot 10^{-7}$ mg and $1.6 \cdot 10^{-12}$ mg at 1,750 rpm. The decreasing trend of ammonia slip as a function of the H_2O_2 share is reasonable because the increase of the H_2O_2 share leads to more intense and complete combustion conditions as was previously discussed in Figs. 4 and 5. The yet greater reduction in the ammonia slip observed at 1,750 rpm is believed to be primarily due to the higher hydrogen share in the initial NH_3/H_2 fuel mix, consistent with what has been previously reported in the literature [44]. Similar to the findings reported in Fig. 3, the ammonia slip values reported in Fig. 8 are significantly lower compared to other studies that used more conventional ammonia-fuelled engine setups, e.g., [36-38], and corroborate further that ammonia slip would most likely not be an issue for the proposed technology over a wide range of operational conditions.

Specific N_2O emissions are similarly negatively correlated with the H_2O_2 share in the directly injected mixture. However, this correlation attenuates with the increase of the H_2O_2 share and appears to level off at sufficiently high H_2O_2 share values, e.g., 0.37 at 750 rpm, 0.40 at 1,250 rpm and 0.33 at 1,750 rpm. Hence, a variation in the specific N_2O emissions between 2,118 and 622 mg/kWh, and between 1,534 and 570 mg/kWh, is demonstrated at 750 and 1,250 rpm, respectively, while at the much higher engine speed of 1,750 rpm this variation is much more limited to between 218 and 3.5 mg/kWh. In fact, at this high speed, N_2O emissions are well below 100 mg/kWh for all H_2O_2 shares higher than 0.3. For reference purposes, when the H_2O_2 share is 0.3, the N_2O emissions are 955, 916 and 63 mg/kWh at 750, 1,250 and 1,750 rpm, respectively. As was already discussed in Fig. 3, a main driver for the N_2O emissions is the combustion temperature (the correlation being a negative one, as also depicted in Fig. 8) and a major reason for these *high* N_2O emissions is the relatively *low* combustion temperature. In fact, Fig. 8 shows that the maximum temperature of the examined cases never exceeds 1,715 K and 1,730 K at 750 and 1,250 rpm, respectively, while at 1,750 rpm the maximum temperature varies between 1,687 K and 1,893 K. As expected, the highest engine speed is associated with much higher combustion temperatures (due to the higher hydrogen share in the mixture) which results in the much lower N_2O emissions (negligibly small in certain cases).

Injection timing and duration analysis

In this last section of the analysis, summarized in Fig. 9, the focus shifts to the effect of different injection strategies. The investigation presented here is neither exhaustive nor optimized against specific outcomes. For example, here only single injections are used in the range of the simulations with uniform injection rates. The results are presented to offer some insight on the response of key variables, such as the developed torque and NO_x emissions, while using the aqueous solution as the pilot fuel. We make the important assumption that the main fuel, *i.e.*, the NH_3/H_2 mixture, exists as a homogenous mixture at the intake BDC. In a future optimization exercise, though, any injection strategy should also include the DI of the NH_3/H_2 mixture. In the current study, the focus is on two key aspects that characterize a pilot injection strategy: the start of injection (SOI) timing and the injection duration (ID) of the pilot fuel. As before, the analysis was conducted at three engine speeds, 750, 1,250 and 1,750 rpm. The SOI varied between -20 and -4 CAD aTDC (750 rpm), -20 and -8 CAD aTDC (1,250 rpm), -20 and -10 CAD aTDC (1,750 rpm). Three injection durations were examined at all engine speeds: 1, 4 and 8 CAD. The mass of the DI solution was maintained at 4.0 mg at 750 and 1,250 rpm and at 8.0 mg at 1,750 rpm and the share of peroxide in the directly injected solution was 30% at all engine speeds. In all cases, the mass of the initial NH_3/H_2 mixture was 105.0 mg; the H_2 share in the initial NH_3/H_2 mixture was kept at 30% at 750 and 1,250 rpm and 40% in the case of 1,750 rpm.

Firstly, looking at 750 rpm, there is no particular conclusion that can be drawn regarding the response of the developed torque against the variation of either the SOI or the ID. This is related to the magnified vertical scale: the average of all the torque results for 750 rpm is 640 Nm, while the standard deviation is 4.7 Nm, i.e., barely 0.7% of the average value. The low standard deviation value clearly indicates how tightly distributed around the mean is the data.

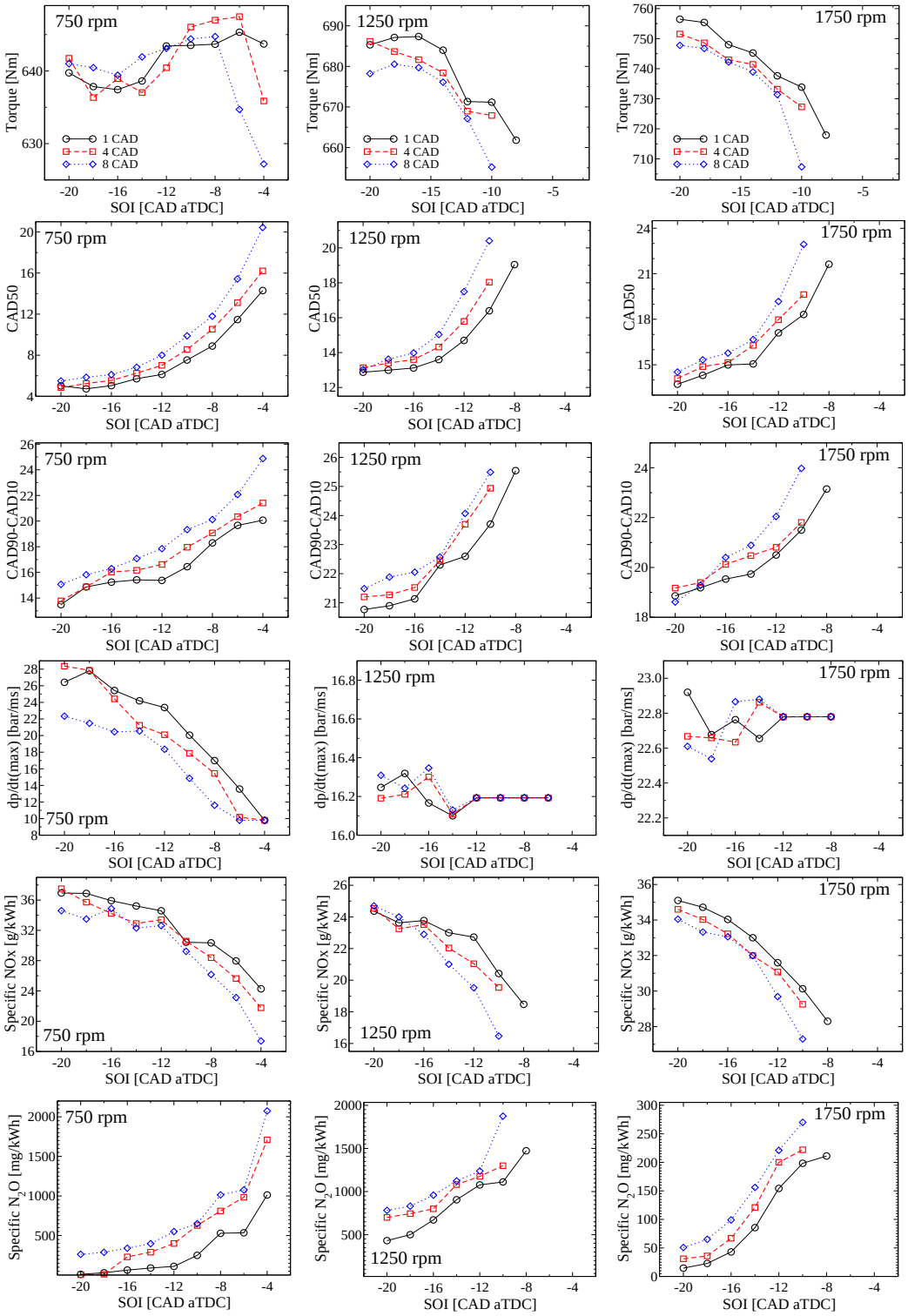

Fig. 9. The change in indicated torque, CAD50, CAD90-CAD10, maximum pressure rise rate, specific NO_x and N_2O as a function of the SOI for three injection durations (ID), 1, 4 and 8 CAD, for three engine speeds: 750, 1,250 and 1,750 rpm. The DI mass of H_2O_2/H_2O mixture was maintained at 4.0 mg at 750 and 1,250 rpm and at 8.0 mg at 1,750 rpm. The hydrogen share was maintained at 30% at 750 and 1,250 rpm and 40% in the case of 1,750 rpm. In all cases, the mass of the initial NH_3/H_2 mixture was 105.0 mg and the share of H_2O_2 in the directly injected diluted mixture was 30%.

Thus, any variation of the torque at 750 rpm is the result of the system's stochasticity. The main reason for this phenomenon is that, at this low engine speed, there is sufficient time for the charge to combust. It must be noted, though, that by retarding the SOI to later than -4 CAD aTDC, the torque drops rapidly because of misfire. Clearer trends emerge by shifting attention to higher engine speeds, 1,250 and 1,750 rpm. There, two major observations can be made: (i) retarding the SOI has an adverse effect on the torque developed; (ii) the longer the ID, the lower the torque developed. Both findings are associated with the system's inability to fully combust and maximise the engine's indicated work; SOI and ID can affect not only the homogeneity of the charge but also the evaporative cooling process which is an important aspect given the pilot fuel's (the aqueous solution) high enthalpy of vaporisation. Notably, misfire was observed for SOI values retarded beyond -8, -10 CAD aTDC for ID 1, 4 and 8 CAD at both engine speeds. It is also worth noting that maximum torque values of 687 Nm (1,250 rpm) and 756 Nm (1,750 rpm) are obtained at SOI/ID -16 CAD aTDC/1 CAD and -20 CAD aTDC/1 CAD, respectively.

Unlike the indicated torque, the responses of the combustion phasing (CAD50) and combustion duration (CAD90-CAD10) to the changes of SOI and ID are evident at all engine speeds. In particular, both CAD50 and the combustion duration tend to decrease with: (i) the advance of the SOI; (ii) the shortening of the ID. The changes in both CAD50 and the combustion duration are not, in principle, linear with the change of SOI. Hence, the impact of changes in the SOI at very advanced times (*i.e.*, earlier than CAD aTDC) on CAD50 are barely noticeable. As the SOI is retarded towards the TDC though, the change of CAD50 becomes more rapid. For example, at 750 rpm, in the case of ID 1 CAD, CAD50 is 5 CAD aTDC when SOI is -20 CAD aTDC and increases to 6.1 CAD aTDC (i.e., 1.1 CAD change) when the SOI is retarded to -12 CAD aTDC (an 8 CAD change). But further retarding the SOI to -10 CAD aTDC (an additional 2 CAD change) leads to CAD50 of 7.5 (1.4 CAD change). This behavior occurs because, at sufficiently advanced SOI times, the mixture has adequate time to mix and build a sufficiently rich radical pool; therefore, any further increase of the mixing time has little impact on the mixture stratification. By retarding the SOI while approaching values close to the TDC, the effect of the SOI in controlling the combustion process becomes progressively more pronounced as it inherently controls the timing and the characteristics of the radical pool formation. This inevitably affects both combustion duration (which tends to become even longer) and CAD50 (which is delayed even further). The same non-linear response is also observed for the combustion duration for the same reasons, although admittedly the flattening of the curve for sufficiently advanced SOI times, that was observed for CAD50, is not found here. Instead, by continuously advancing the SOI, the combustion duration will in principle continue decreasing, yet the rate of this decrease will become less pronounced. Another finding that needs to be reported is that the effect of the ID, particularly in view of CAD50, becomes more notable as the SOI is delayed. For example, in the case of 1,250 rpm, CAD50 is 12.9, 13.1, 13 when the SOI is -20 CAD aTDC for ID of 1, 4, 8 CAD, respectively, but when the SOI is retarded to -10 CAD aTDC, the respective values become 16.4, 18.3, 20.4. The reason for this response is due to the combined effect of the SOI and ID on the radical pool build-up. In particular, the examination of the molar concentrations of key radicals like OH and H showed that their maximum values decrease with the retarding of the SOI or the increase of the ID. In fact, the effect of the ID on the radical pool generation becomes more pronounced for SOI values closer to the TDC. This is reasonable because as the SOI moves closer to the TDC, it allows progressively less time for the charge to fully combust. By increasing the ID, the time taken for the pilot fuel to enter the cylinder and mix with the charge – thereby allowing it to act as an ignition source - is enhanced, hence the combustion process is retarded further thereby leading to a gradually diminished radical pool.

The maximum pressure rise rate exhibits some meaningful response only for the case of 750 rpm. For the other two engine speeds, 1,250 and 1,750 rpm, the change of the maximum pressure rise rate as a function of either the SOI or the ID is negligibly small and varies in a stochastic manner. In contrast, in the case of 750 rpm, the maximum pressure rise rate varies substantially from 9.8 bar/ms (SOI: -4 CAD aTDC, ID: 8 CAD) up to 28.4 bar/ms (SOI: -20 CAD aTDC, ID: 4 CAD). It is worth highlighting that all these values are well below the threshold of 50 bar/ms to ensure a safe and smooth engine operation. In order to get an insight into the different response of the maximum pressure rise rate that is observed at the different speeds, we need to consider the combustion timing and duration. Naturally, the closer to the TDC that ignition occurs, and the shorter the combustion duration, the more intense the combustion event, *i.e.*, the greater the pressure

rise rate. Let us consider a straight horizontal line that crosses the y-axis at 13 CAD aTDC in the CAD50 figure for 750 rpm. It is noticed that most of the CAD50 results (for all three cases of ID in the case of 750 rpm) are below that straight line (i.e. more advanced). Only the two cases of SOI of -4 aTDC (for all three ID values) and SOI -6 CAD aTDC (ID:8 CAD) give values of CAD50 above 13 CAD aTDC (*i.e.*, more retarded). In the case of 1,250 rpm, the faster CAD50 values (*i.e.*, more advanced) are marginally higher than 13 CAD aTDC, while at 1,750 rpm CAD50 is always well above (*i.e.*, more retarded) 13 CAD aTDC. The cases that exhibit more advanced CAD50 than 13 CAD aTDC at 750 rpm (*i.e.*, most of the cases at 750 rpm) are characterised by combustion duration ranging between 13 and 20 CAD. However, at 1,250 rpm, the combustion duration varies between 20.5 and 25 CAD, *i.e.*, much longer than the combustion duration characterised at 750 rpm. Similarly, at 1,750 rpm the combustion duration varies between 18.5 and 24 CAD. So, at 1,250 and 1,750 rpm either the ignition timing is much retarded in the power stroke compared to what happens at 750 rpm, or the combustion duration is much longer, or, in most cases, both occur. This results in more intense combustion events at 750 rpm as manifested by the behaviour of the maximum pressure rise rate.

The last part of this analysis concerns the variation of NO_x and N_2O emissions as a function of the SOI and the ID for the three engine speeds. From the results in Fig. 9 the following observations can be made: (1) at all speeds, specific NO_x emissions fall while N_2O emissions increase with retarding the SOI; (2) in principle, the increase of the ID leads to the decrease of specific NO_x and the increase of N_2O emissions; (3) depending on the combination of SOI and ID, the impact of retarding SOI can be stronger or weaker than ID in reducing NO_x and N_2O emissions; (4) the specific NO_x values range between 17.3-37.5 g/kWh (750 rpm), 16.5-24.7 g/kWh (1,250 rpm), 27.3-35.1 g/kWh (1,750 rpm); (5) specific N_2O emissions have a much wider range of variation compared to NO_x, ranging between 10-2,073 mg/kWh (750 rpm), 431-1,875 mg/kWh (1,250 rpm), 15-270 mg/kWh (1,750 rpm). It is, as expected, that N_2O emissions have the opposite trend to NO_x emissions, both as a function of the SOI and the ID. As explained earlier, the more advanced the ignition time (represented by CAD50) bringing it closer to TDC, and the shorter the combustion duration (CAD90-CAD10), the more intense the combustion event, which is reflected in faster (and higher) development of pressures. The higher pressures inherently also mean higher temperatures. Since earlier we have established the connection and strong correlation between maximum temperature and NO_x/N_2O emissions, it is then natural to expect that as the maximum temperature increases so will the NO_x emissions, but N_2O emissions will drop; thereby explaining observations (1) and (2). When the SOI is sufficiently advanced (e.g., -18 CAD aTDC), the DI solution has more time available to mix with the premixed NH_3/H_2/air charge, thereby allowing combustion to reach higher temperatures. Consequently, tweaking the SOI or ID at these conditions has little impact on the combustion process as was also confirmed by the profiles of CAD50 and CAD90-CAD10. However, as the SOI is retarded, the response of NO_x and N_2O emissions to the change of SOI or ID becomes more pronounced in alignment with the response of CAD50 and the combustion duration that was reported earlier at these conditions. Regarding the ranges of specific NO_x values reported for the three engine speeds, all these values exceed the IMO's Tier III standards by a factor of, between 5 and 10. Finally, the N_2O emissions reported in Fig. 9 are mostly relatively high, consistent with what was reported earlier in Figs. 3 and 8. However, Fig. 9 demonstrates that low N_2O emission values (i.e., below 150 mg/kWh) can be obtained with a combination of very early SOI and short ID. For example, both at 750 and 1,750 rpm, an injection duration of 1 CAD enables low N_2O emissions when the SOI is -12 CAD aTDC or earlier. It is noted, though, that under the investigated conditions, no combination of early SOI and short ID could lead to low N_2O emissions at 1,250 rpm, which merely indicates that N_2O emissions reduction must be considered in any optimisation exercise that will span a range of engine speeds.

Conclusions

The current study is a first attempt to explore the use of an aqueous solution of hydrogen peroxide as pilot fuel, at weight concentrations which are readily commercially available, in a CI engine fuelled by a premixed charge of NH_3/H_2 at intake BDC without preheating the air or NH_3/H_2/air charge. We have employed an advanced stochastic engine computational model for this purpose that accounted for: (i) detailed chemistry including NO_x; (ii) heat transfer to the engine cylinder wall; (iii) in-cylinder mixture and temperature inhomogeneities; (iv) the direct injection of the pilot fuel; (iv) the evaporation process of the pilot fuel. The analysis extends over a wide range of engine speeds (750 – 1,750 rpm) and

focuses on three aspects: (i) engine performance; (ii) combustion phasing; (iii) NO_x emissions. These three aspects are investigated with: (i) the variation of the mass (0.1-10 mg) of the directly injected (DI) peroxide solution; (ii) the variation of the H_2O_2 share (15-50%) in the directly injected (DI) peroxide solution; (iii) the variation of the start of injection (from -20 to -4 CAD aTDC) and injection duration (1-8 CAD). We emphasize that, for most cases and on a volume basis, the required aqueous H_2O_2 pilot amount is only 3% of the main fuel, while on an energy basis this translates to only 1.1% of the main fuel blend.

In the first part of the study, the increase of the DI mass of solution leads to the advance of CAD50 and higher pressures which, combined, result in higher work output and torque. The maximum indicated torques of 655 Nm, 691 Nm and 745 Nm were achieved at engine speeds of 750, 1,250 and 1,750 rpm, respectively. On average (considering all engine speeds) the maximum indicated thermal efficiency was 0.51. The increase of the DI mass of the solution had a strong effect on combustion phasing and particularly on CAD50 which decreased by 48%, 44% and 33% (10.4, 10.8 and 16.1 CAD) relative to minimum required H_2O_2 share at engine speeds of 750, 1,250 and 1,750 rpm, respectively. The effect was notable on the combustion duration as well, resulting in values between 4.5 and 7.7 CAD, depending on the engine speed. The maximum pressure rise rate increased with the increase of the DI mass of the solution, but with most values below 28.5 bar/ms. NO_x emissions increased with the increase of the DI mass of the solution, because of the increase of the in-cylinder temperature, with values between 18 – 34 g/kWh, depending on the engine speed. The unburned ammonia ("slip") ratio was found to be negligibly low in all examined cases, reaching a maximum of 0.7%. On the other hand, N_2O emissions ranged between 54-1,477 mg/kWh and were found to decrease with the increase of the hydrogen share. Also, there is a negative correlation between the maximum temperature and N_2O emissions (in agreement with the literature): the relatively low combustion temperatures prevailing in the conditions of these calculations explain the relatively high N_2O emissions that we report.

In the second part of the study, we analysed the effect of the H_2O_2 share in the aqueous solution (from 10% up to 50%). The introduction of H_2O_2 strongly favors the enhancement of the radical pool generation, although there is no effect on reactant temperature by the end of injection. Subsequently, we find a (decreasing) linear correlation between CAD50 and OH radical concentration for the examined conditions. Furthermore, an increase of the H_2O_2 concentration decreases the solution's enthalpy of evaporation, as the value for H_2O_2 is more than 4 times higher than that of diesel, thereby leading to a cooling effect during its direct injection which moderates the temperature increase after the completion of the direct injection. The effect of the H_2O_2 share increases the indicated torque: maximum values of 651, 691 Nm and 765 Nm were reported for engine speeds of 750, 1,250 and 1,250 rpm, respectively. Using a H_2O_2/H_2O mixture with 30% H_2O_2 share, the indicated thermal efficiency ranged between 0.489 and 0.519, depending on the engine speed. The ignition advance achieved by the increase of the H_2O_2 share (from 15% to 25% at 750 rpm) was accompanied by a combustion duration which was shorter by more than 25% (from 27 to 20 CAD). Using a 30% H_2O_2 share resulted in maximum pressure rise rates of between 10.3 and 24.4 bar/ms for all engine speeds. Caution is needed for mixtures with greater than 40% H_2O_2 share because these can potentially lead to excessive (>50 bar/ms) maximum pressure rise rates. As expected, there is a linear correlation between specific NO_x emission and maximum temperature. In general, specific NO_x values ranged between 14.6 and 40.9 g/kWh for all engine speeds. The ammonia slip ratio was, once again, consistently extremely low, reaching a maximum of 0.73% in the worst case. On the other hand, N_2O emissions were consistently high at low-medium engine speeds (570 - 2,118 mg/kWh) although at the highest engine speed these emissions dropped significantly to mostly low values, mainly due to the higher hydrogen share in the fuel mix.

In the third and last part of the study, the start of injection (SOI) and the injection duration (ID) were both varied, from -20 to -4 CAD aTDC for the former and 1 to 8 CAD for the latter. Retarding the SOI, and longer IDs, resulted in lower indicated torque. Both CAD50 and the combustion duration tended to advance and decrease, respectively, with either advancing the SOI or shortening the ID. The maximum pressure rise rate varied little with SOI or ID at higher engine speeds but, at the low engine speed of 750 rpm, values decreased from 28.4 to 9.4 bar/ms with either retarding the SOI or the prolonging the ID. The NO_x emissions reduced with the retarding the SOI or increasing the ID and varied between 16.5 and 37.5 g/kWh for all engine speeds. The N_2O emissions exhibited an opposite trend to

that of the NO_x, increasing with the retarding of the SOI or the increase of the ID. Although N_2O emissions exhibited a wide range of variation (10-2,073 mg/kWh accounting for all engine speeds), the results indicated a potential for low N_2O emissions (below 150 mg/kWh) at some engine speeds (750 and 1,750 rpm) when using a combination of short ID (1 CAD) and early SOI (-12 CAD aTDC or earlier).

The results reported herein are promising and make a case for the need for further research, particularly for experiments that will ultimately provide a proof of concept of the proposed technology. Two of the challenges that were identified in the current work were that the production of NO_x emissions exceeded the IMO's Tier III standard and N_2O emissions reached relatively high values (in certain cases well above 150 mg/kWh). Possible ways to tackle NO_x emissions would be the use of exhaust gas recirculation, the use of aftertreatment, and the optimisation of the injection strategy. For the N_2O emissions, on the other hand, different injection strategies should be investigated, possibly with multiple injections. The use of some catalytic aftertreatment may also be necessary to alleviate the increased N_2O emissions as an alternative. Another aspect that requires investigation is the effect of direct injection of both the main fuel, i.e., NH_3/H_2, and the peroxide solution to produce a suitable mixture of ammonia and hydrogen before pilot injection. Finally, although the current study was performed while keeping the inlet temperature to the minimum, thereby requiring a significant amount of hydrogen in the main fuel mix, future studies may be warranted to investigate the trade-off on the engine operation between inlet preheating and hydrogen share in the fuel mixture.

Acknowledgments

None

Conflicts of Interest

The authors declare no conflict of interest.

References

1. Li T, Duan Y, Wang Y, Zhou M, Duan L. Research progress of ammonia combustion toward low carbon energy. Fuel Process. Technol. 2023; 248: 107821. https://doi.org/10.1016/j.fuproc.2023.107821
2. Kang L, Pan W, Zhang J, Wang W, Tang C. A review on ammonia blends combustion for industrial applications. Fuel 2023; 332: 126150. https://doi.org/10.1016/j.fuel.2022.126150
3. Guiberti TF, Pezzella G, Hayakawa A, Sarathy SM. Mini Review of Ammonia for Power and Propulsion: Advances and Perspectives. Energy Fuels 2023; 37(19): 14538-14555. https://doi.org/10.1021/acs.energyfuels.3c01897
4. Chiong MC, Chong CT, Ng JH, Mashruk S, Chong WWF, Samiran NA, Mong GR, Valera-Medina A. Advancements of combustion technologies in the ammonia-fuelled engines. Energy Convers. Manag. 2021; 244: 114460. https://doi.org/10.1016/j.enconman.2021.114460
5. Tornatore C, Marchitto L, Sabia P, De Joannon M. Ammonia as green fuel in internal combustion engines: state-of-the-art and future perspectives. Front. Mech. Eng. 2022; 72. https://doi.org/10.3389/fmech.2022.944201
6. Chiong MC, Kang HS, Shaharuddin NMR, Mat S, Quen LK, Ten KH, Ong MC. Challenges and opportunities of marine propulsion with alternative fuels. Renew. Sust. Energ. Rev. 2021; 149: 111397. https://doi.org/10.1016/j.rser.2021.111397
7. Aakko-Saksa PT, Lehtoranta K, Kuittinen N, Järvinen A, Jalkanen JP, Johnson K, Jung H, Ntziachristos L, Gagné, S, Takahashi C, Karjalainen P, Timonen H. Reduction in greenhouse gas and other emissions from ship engines: Current trends and future options. Prog. Energy Combust. Sci. 2023; 94: 101055. https://doi.org/10.1016/j.pecs.2022.101055
8. Karvounis P, Tsoumpris C, Boulougouris E, Theotokatos G. Recent advances in sustainable and safe marine engine operation with alternative fuels. Front. Mech. Eng. 2022; 8: 994942. https://doi.org/10.3389/fmech.2022.994942
9. Tingas E.-A, Taylor AM. 2023. Hydrogen: Where it Can Be Used, How Much is Needed, What it May Cost (pp. 3-64). In Hydrogen for Future Thermal Engines, Ed. E.A-. Tingas . Cham: Springer International Publishing. https://doi.org/10.1007/978-3-031-28412-0_1
10. Dimitriou P, Javaid R. A review of ammonia as a compression ignition engine fuel. Int. J. Hydrog. Energy 2020; 45(11): 7098-7118. https://doi.org/10.1016/j.ijhydene.2019.12.209
11. Truedsson I, Foucher F, Pochet M, Jeanmart, H, Contino F. Ammonia-hydrogen blends in homogeneous-charge compression-ignition engine. SAE Technical Paper 2017: No. 2017-24-0087. https://doi.org/10.1016/j.ijhydene.2019.12.209
12. Pochet M, Jeanmart H, Contino F. A 22:1 compression ratio ammonia-hydrogen HCCI engine: combustion, load, and emission performances, Front. Mech. Eng. 2020; 6: 43. https://doi.org/10.3389/fmech.2020.00043
13. Wang B, Yang C, Wang H, Hu D, Duan B, Wang Y. Study on injection strategy of

ammonia/hydrogen dual fuel engine under different compression ratios, Fuel 2023; 334: 126666. https://doi.org/10.1016/j.fuel.2022.126666

14. Wang B, Wang H, Duan B, Yang C, Hu, D, Wang Y. Effect of ammonia/hydrogen mixture ratio on engine combustion and emission performance at different inlet temperatures, Energy 2023; 272: 127110. https://doi.org/10.1016/j.energy.2023.127110

15. Kurien C, Mittal M. Review on the production and utilization of green ammonia as an alternate fuel in dual-fuel compression ignition engines. Energy Convers. Manag. 2022; 251: 114990. https://doi.org/10.1016/j.enconman.2021.114990

16. Wang B, Yang C, Wang H, Hu D, Wang Y. Effect of diesel-ignited ammonia/hydrogen mixture fuel combustion on engine combustion and emission performance, Fuel 2023; 331: 125865. https://doi.org/10.1016/j.fuel.2022.125865

17. Wang H, Wang B, Yang C, Hu D, Duan B, Wang Y. Study on dual injection strategy of diesel ignition ammonia/hydrogen mixture fuel engine, Fuel 2023; 248: 128526. https://doi.org/10.1016/j.fuel.2023.128526

18. Krishna M. Experimental investigation on CI engine with hydrogen peroxide as an alternate, Glob. J. Res. Eng. 2020; 20(1): 37-41. https://engineeringresearch.org/index.php/GJRE/article/view/2004

19. Fanz B, Roth P. Injection of a H2O2/water solution into the combustion chamber of a direct injection diesel engine and its effect on soot removal, Proc. Combust. Inst. 2000; 28: (1) 1219–1225. https://doi.org/10.1016/S0082-0784(00)80333-1

20. Yeom J-K, Jung S-H, Yoon J-H. An experimental study on the application of oxygenated fuel to diesel engines, Fuel 2019; 248: 262–277. https://doi.org/10.1016/j.fuel.2018.12.131

21. Fernie O, Megaritis T, Ganippa LC, Tingas E-A. Numerical analysis of zero-carbon HCCI engine fuelled with steam diluted H2/H2O2 blends, Fuel 2022; 326: 125100. https://doi.org/10.1016/j.fuel.2022.125100

22. Dimitrova ID, Megaritis T, Ganippa LC, Tingas E- A. Computational analysis of an HCCI engine fuelled with hydrogen/hydrogen peroxide blends, Int. J. Hydrog. Energy 2022; 47 (17): 10083–10096. https://doi.org/10.1016/j.ijhydene.2022.01.093

23. Zhou A, Zhang C, Li Y, Li S, Yin P. Effect of hydrogen peroxide additive on the combustion and emission characteristics of an n-butanol homogeneous charge compression ignition engine, Energy 2019; 169: 572–579. https://doi.org/10.1016/j.energy.2018.12.076

24. Shafiq O, Tingas E-A. Computational investigation of ammonia-hydrogen peroxide blends in HCCI engine mode, Int. J. Engine Res. 2023; 24 (5): 2279–2294. https://doi.org/10.1177/14680874221117686

25. Yang W, Al Khateeb AN, Kyritsis DC. The effect of hydrogen peroxide on NH3/O2 counterflow diffusion flames, Energies 2022; 15 (6): 2216. https://doi.org/10.3390/en15062216

26. Cordiner S, Gambino M, Iannaccone S, Rocco V, Scarcelli R. Numerical and experimental analysis of combustion and exhaust emissions in a dual-fuel diesel/natural gas engine, Energy Fuels 2008; 22 (3): 1418–1424. https://doi.org/10.1021/ef7004755

27. Saxena MR, Maurya RK. Exergy analysis and investigation on effect of inlet valve closing temperature and hydrogen enrichment in syngas composition in an HCCI engine, Int. J. Hydrogen Energy 2023; 48 (8): 3269–3286. https://doi.org/10.1016/j.ijhydene.2022.10.123

28. Coskun G, Demir U, Soyhan HS, Turkcan A, Ozsezen AN, Canakci M. An experimental and modelling study to investigate effects of different injection parameters on a direct injection HCCI combustion fueled with ethanol–gasoline fuel blends, Fuel 2018; 215: 879–891. https://doi.org/10.1016/j.fuel.2017.11.126

29. Yasar H, Usta E, Demir U. Experimental and stochastic reactor modeling results of an HCCI engine fueled with primary reference fuel, Energy Fuels 2018; 32 (2): 2497–2505. https://doi.org/10.1021/acs.energyfuels.7b03880

30. Pasternak M, Mauss F, Perlman C, Lehtiniemi, H. Aspects of 0D and 3D modelling of soot formation for diesel engines, Combust. Sci. Technol. 2014; 186 (10-11): 1517–1535. https://doi.org/10.1080/00102202.2014.935213

31. CMCL Innovations UK, Kinetics & SRM Engine Suite, v 21 (2021).

32. Pope SB. PDF methods for turbulent reactive flows, Prog. Energy Combust. Sci. 1985; 11(2): 119–192. https://doi.org/10.1016/0360-1285(85)90002-4

33. Maurya RK, Akhil N. Development of a new reduced hydrogen combustion mechanism with NO_x and parametric study of hydrogen HCCI combustion using stochastic reactor model, Energy Convers. Manag. 2017; 132: 65–81. https://doi.org/10.1016/j.enconman.2016.11.021

34. Zhang, X.; Moosakutty, S.P.; Rajan, R.P.; Younes, M.; Sarathy, S.M. Combustion chemistry of ammonia/hydrogen mixtures: Jet-stirred reactor measurements and comprehensive kinetic modelling, Combust. Flame 2021; 234: 111653. https://doi.org/10.1016/j.combustflame.2021.111653

35. Maurya RK, Mishra P. Parametric investigation on combustion and emissions characteristics of a dual fuel (natural gas port injection and diesel pilot injection) engine using 0-

D SRM and 3D CFD approach, Fuel 2017; 210: 900–913. https://doi.org/10.1016/j.fuel.2017.09.021

36. Yousefi A, Guo H, Dev S, Liko B, Lafrance S. Effects of ammonia energy fraction and diesel injection timing on combustion and emissions of an ammonia/diesel dual-fuel engine. Fuel 2022; 314: 122723. https://doi.org/10.1016/j.fuel.2021.122723

37. Chen R, Li T, Wang X, Huang S, Zhou X, Li S, Yi P. Engine-out emissions from an ammonia/diesel dual-fuel engine–The characteristics of nitro-compounds and GHG emissions. Fuel 2024; 362: 130740. https://doi.org/10.1016/j.fuel.2023.130740

38. Bjørgen KOP, Emberson DR, Løvås T. Combustion of liquid ammonia and diesel in a compression ignition engine operated in high-pressure dual fuel mode. Fuel 2024; 360: 130269. https://doi.org/10.1016/j.fuel.2023.130269

39. Qi Y, Liu W, Liu S, Wang W, Peng Y, Wang Z. A review on ammonia-hydrogen fueled internal combustion engines. eTransportation 2023: 100288. https://doi.org/10.1016/j.etran.2023.100288

40. Mathieu O, Petersen EL. Experimental and modeling study on the high-temperature oxidation of Ammonia and related NO_x chemistry. Combust. Flame 2015; 162(3): 554-570. https://doi.org/10.1016/j.combustflame.2014.08.022

41. Chen R, Li T, Wang X, Huang S, Zhou X, Li S, Yi P. Engine-out emissions from an ammonia/diesel dual-fuel engine–The characteristics of nitro-compounds and GHG emissions. Fuel 2024; 362: 130740. https://doi.org/10.1016/j.fuel.2023.130740

42. Wu B, Wang Y, Wang D, Feng Y, Jin S. Generation mechanism and emission characteristics of N_2O and NO_x in ammonia-diesel dual-fuel engine. Energy 2023; 284: 129291. https://doi.org/10.1016/j.energy.2023.129291

43. Nadimi E, Przybyła G, Lewandowski MT, Adamczyk W. Effects of ammonia on combustion, emissions, and performance of the ammonia/diesel dual-fuel compression ignition engine. J. Energy Inst. 2023; 107: 101158. https://doi.org/10.1016/j.joei.2022.101158

44. Zhu T, Yan X, Gao Z, Qiu Y, Zhu L, Huang Z. Combustion and emission characteristics of ammonia-hydrogen fueled SI engine with high compression ratio. Int. J. Hydrog. Energy 2024;. 62: 579-590. https://doi.org/10.1016/j.ijhydene.2024.03.035